iScience, Volume *26*

Supplemental information

Direct assessment of nitrative stress in lipid environments: Applications of a designer lipid-based biosensor for peroxynitrite

Bryan Gutierrez, Tushar Aggarwal, Huseyin Erguven, M. Rhia L. Stone, Changjiang Guo, Alyssa Bellomo, Elena Abramova, Emily R. Stevenson, Debra L. Laskin, Andrew J. Gow, and Enver Cagri Izgu

Supplemental Information for

Direct Assessment of Nitrative Stress in Lipid Environments: Applications of a Designer Lipid-Based Biosensor for Peroxynitrite

Bryan Gutierrez[1‡], Tushar Aggarwal[1‡], Huseyin Erguven[1], M. Rhia L. Stone[1], Changjiang Guo[2], Alyssa Bellomo[2], Elena Abramova[2], Emily R. Stevenson[2], Debra L. Laskin[2], Andrew J. Gow[2], and Enver Cagri Izgu[1,3,4 *]

(1) Department of Chemistry and Chemical Biology, Rutgers University, New Brunswick, NJ 08854, USA

(2) Ernest Mario School of Pharmacy, Department of Pharmacology & Toxicology, Rutgers University, New Brunswick, NJ 08901, USA

(3) Cancer Institute of New Jersey, Rutgers University, New Brunswick, NJ 08901, USA

(4) Rutgers Center for Lipid Research, New Jersey Institute for Food, Nutrition, and Health, Rutgers University, New Brunswick, NJ 08901, USA

[‡]These authors contributed equally

*Corresponding author: Enver Cagri Izgu (ec.izgu@rutgers.edu)

Chemicals

Reagents: 1-2-dipalmitoyl-*rac*-glycerol, pyridine, and 7 M ammonium hydroxide, triethylamine (TEA), dimethyl sulfoxide [(DMSO), molecular biology grade], copper (II) sulfate ($CuSO_4$), 2-{2-[2-(2-propynyloxy)ethoxy]-ethoxy}ethanol, hydrogen peroxide (H_2O_2), sodium hydroxide (NaOH), sodium nitrite ($NaNO_2$), potassium superoxide (KO_2), sodium ascorbate, 1,1,1-trifluoro-4-(4-hydroxyphenyl)butan-2-one, triphosgene, Oxone, sucrose, ethylene chlorophosphite, triphenylphosphine oxide (Ph_3PO), sodium bicarbonate ($NaHCO_3$), Coumarin 343, and sodium sulfate (Na_2SO_4) were purchased from Millipore-Sigma. 3-azido-7-hydroxycoumarin was purchased from Biosynth International Inc. Tris(3-hydroxypropyltriazolyl-methyl)amine (THPTA) was purchased from Click Chemistry Tools. 1-Palmitoyl-2-oleoyl-*sn*-glycero-3-phosphocholine (POPC), 1,2-palmitoyl-*sn*-glycero-3-phosphocholine (DPPC), and 1,2-dioleoyl-*sn*-glycero-3-phosphoethanolamine-*N*-(lissamine rhodamine B sulfonyl) (ammonium salt) (here referred to as Liss-Rhod PE) were purchased from Avanti Polar Lipids. 3-(4,5-Dimethylthiazol-2-yl)-2,5-diphenyl tetrazolium bromide (MTT) cell proliferation assay kit was purchased from ATCC.

Buffers, Solvents, Media: Phosphate-buffered saline (PBS), 4-morpholineethanesulfonic acid (MES), tris(hydroxymethyl)aminomethane (Tris), dichloromethane (CH_2Cl_2), ethyl acetate (EtOAc), benzene, toluene, tetrahydrofuran (THF), and chloroform ($CHCl_3$) were purchased from Millipore Sigma. Acetonitrile (CH_3CN) and methanol (MeOH, HPLC grade) were purchased from Fisher Scientific. Deuterated solvents were purchased from either Cambridge Isotope Laboratories or Millipore Sigma. Deuterated solvents contained 0.05% (v/v) TMS as a secondary internal reference. Water was deionized and filtered to a resistivity of 18.2 ΩM with a Milli-Q® Plus water purification system (Millipore, Massachusetts). Buffers were prepared freshly in Milli-Q® water and their pH were adjusted using HCl or NaOH using a Thermo Scientific Orion Star pH meter. Dulbecco's Modified Eagle Medium (DMEM) with and without phenol red was purchased from Corning. Hanks' Balanced Salt Solution (HBSS) and fetal bovine serum (FBS) were purchased from VWR International.

Chemicals used for the animal work were outlined in Key Resource Table in the main manuscript.

Note that the hazardous chemicals used in this study, especially triphosgene, nitrogen mustard, bleomycin, ketamine, xylazine, and volatile solvents were handled using the necessary protective gears and according to the guidelines of Rutgers Environmental Health and Safety.

Data S1: ^{1}H, ^{13}C, ^{19}F, and ^{31}P NMR spectra of compounds, related to STAR Methods

Compound ***3*** (^{1}H NMR: 500 MHz, $CDCl_3$)

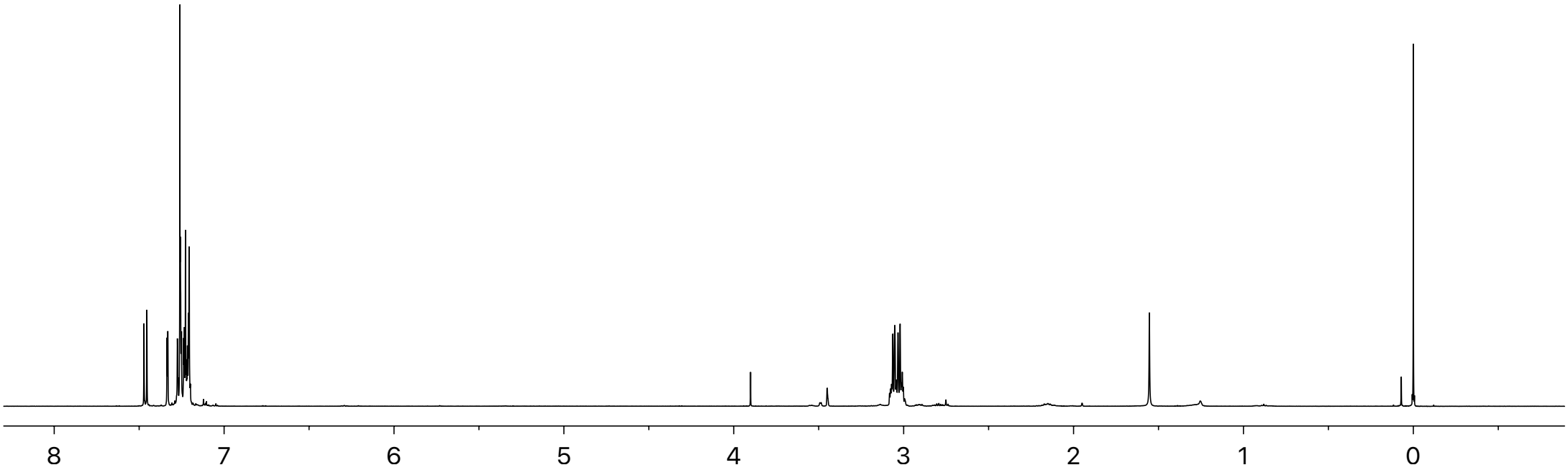

Compound ***3*** (^{13}C NMR: 126 MHz, $CDCl_3$)

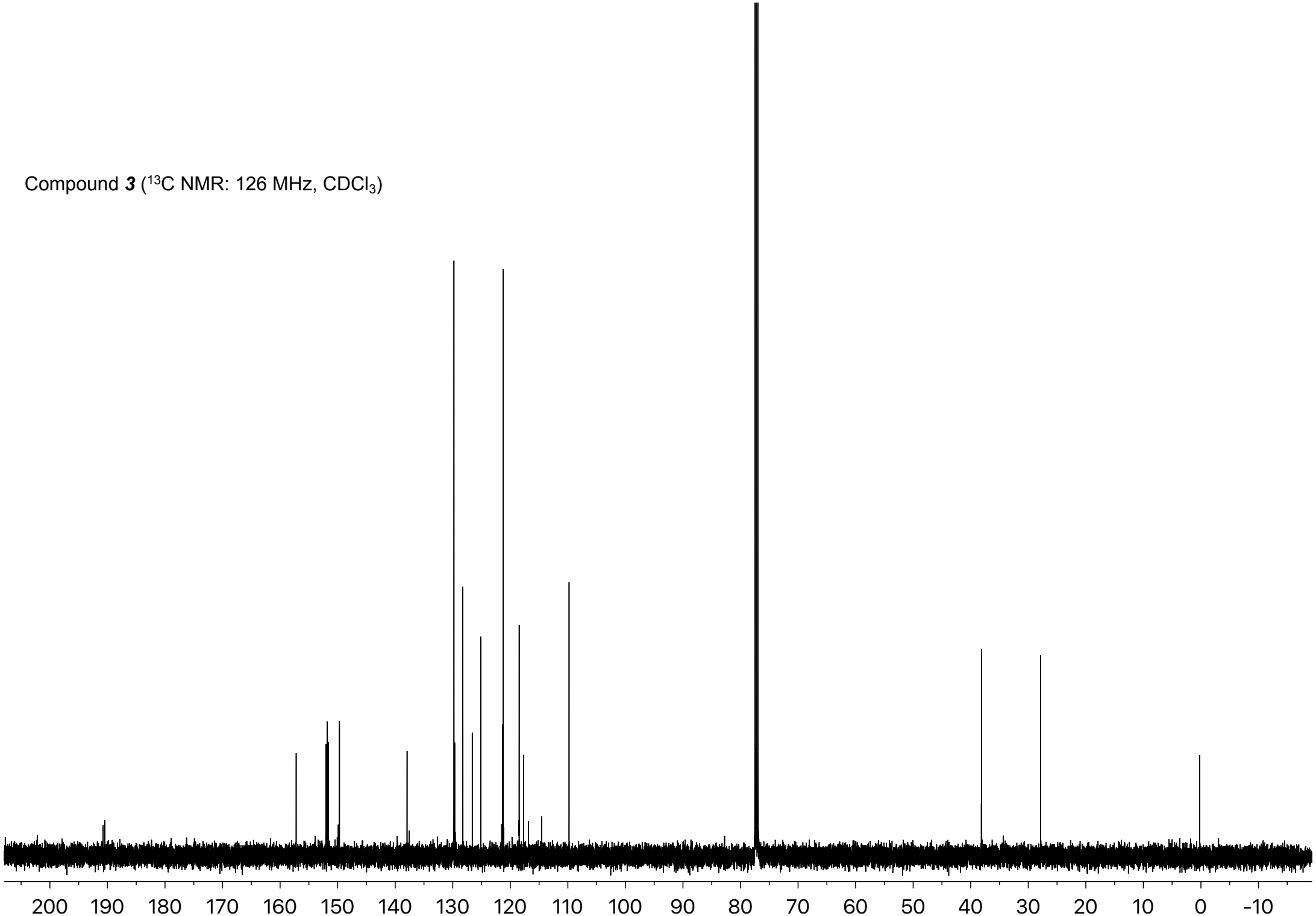

Compound ***3*** (^{19}F NMR: 471 MHz, $CDCl_3$)

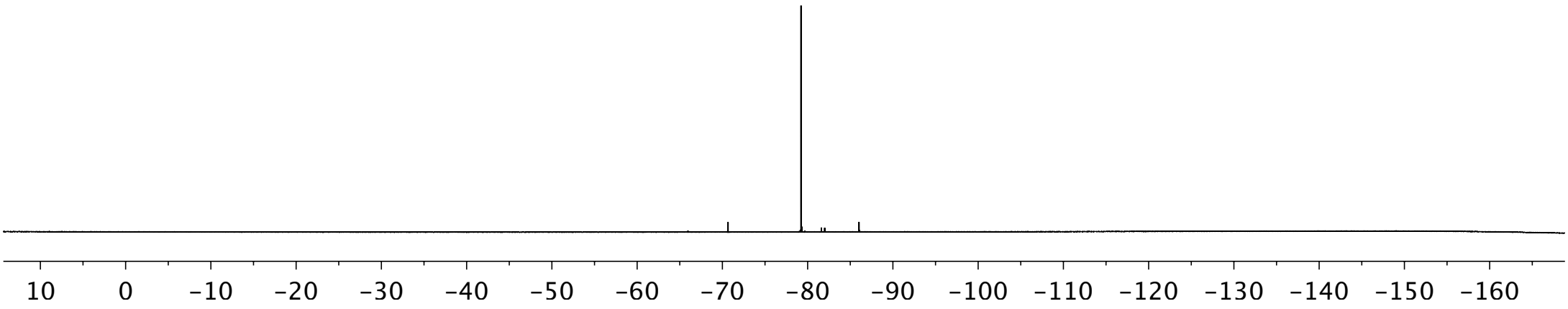

TEG-TC-ONOO^{-} (^{1}H NMR: 500 MHz, $CDCl_3$))

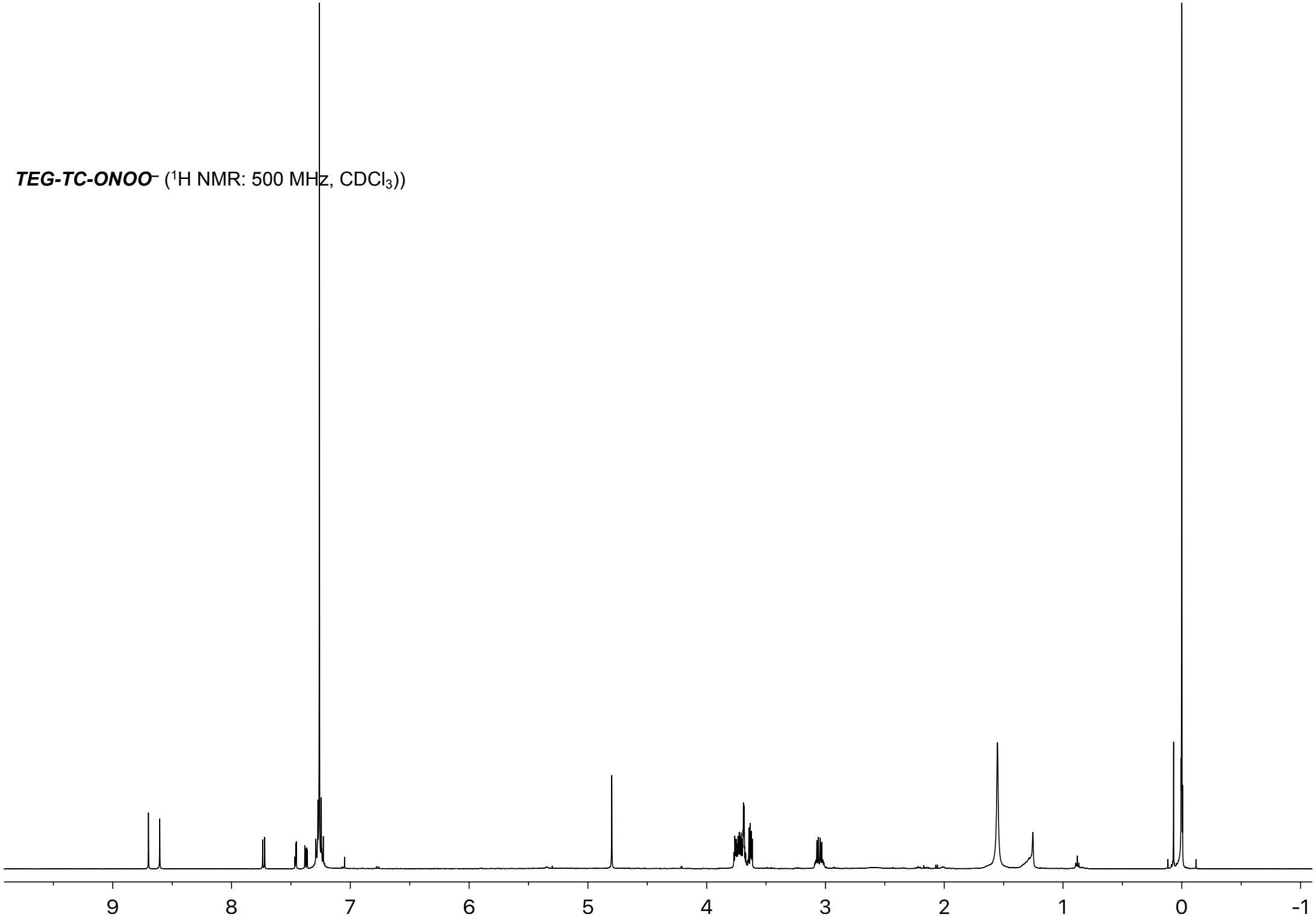

TEG-TC-ONOO $^{-}$ (^{13}C NMR: 126 MHz, $CDCl_3$)

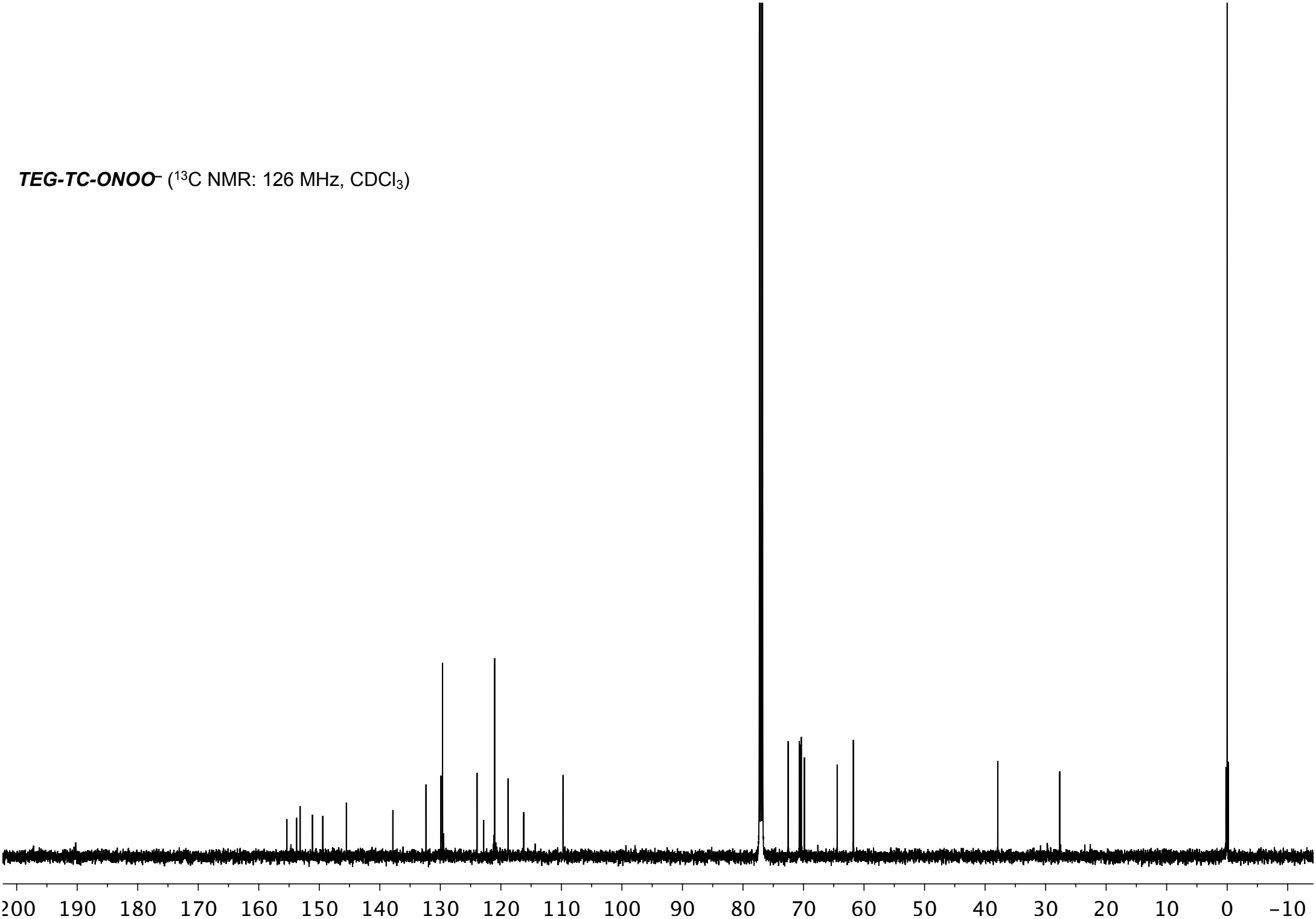

TEG-TC-ONOO $^{-}$ (^{19}F NMR: 471 MHz, $CDCl_3$)

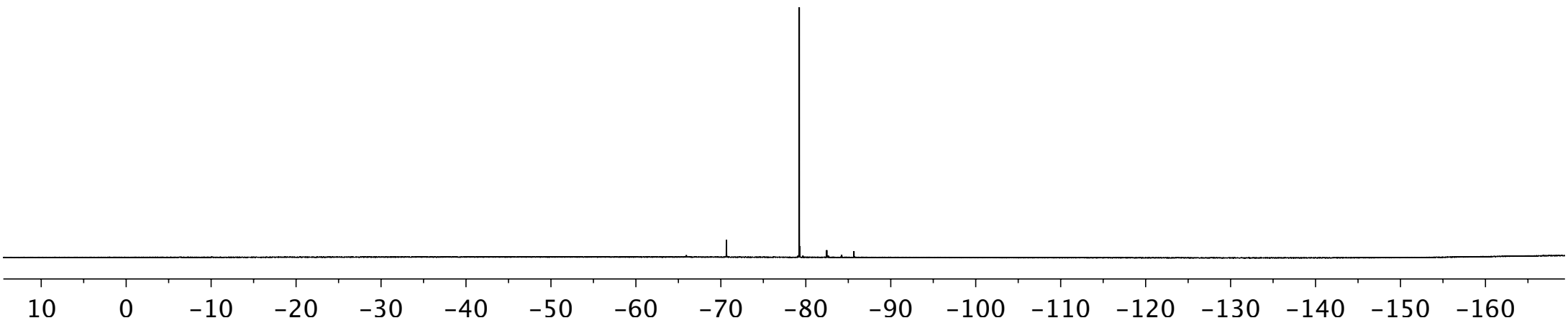

Compound ***S2*** (^{1}H NMR: 500 MHz, $CDCl_3$)

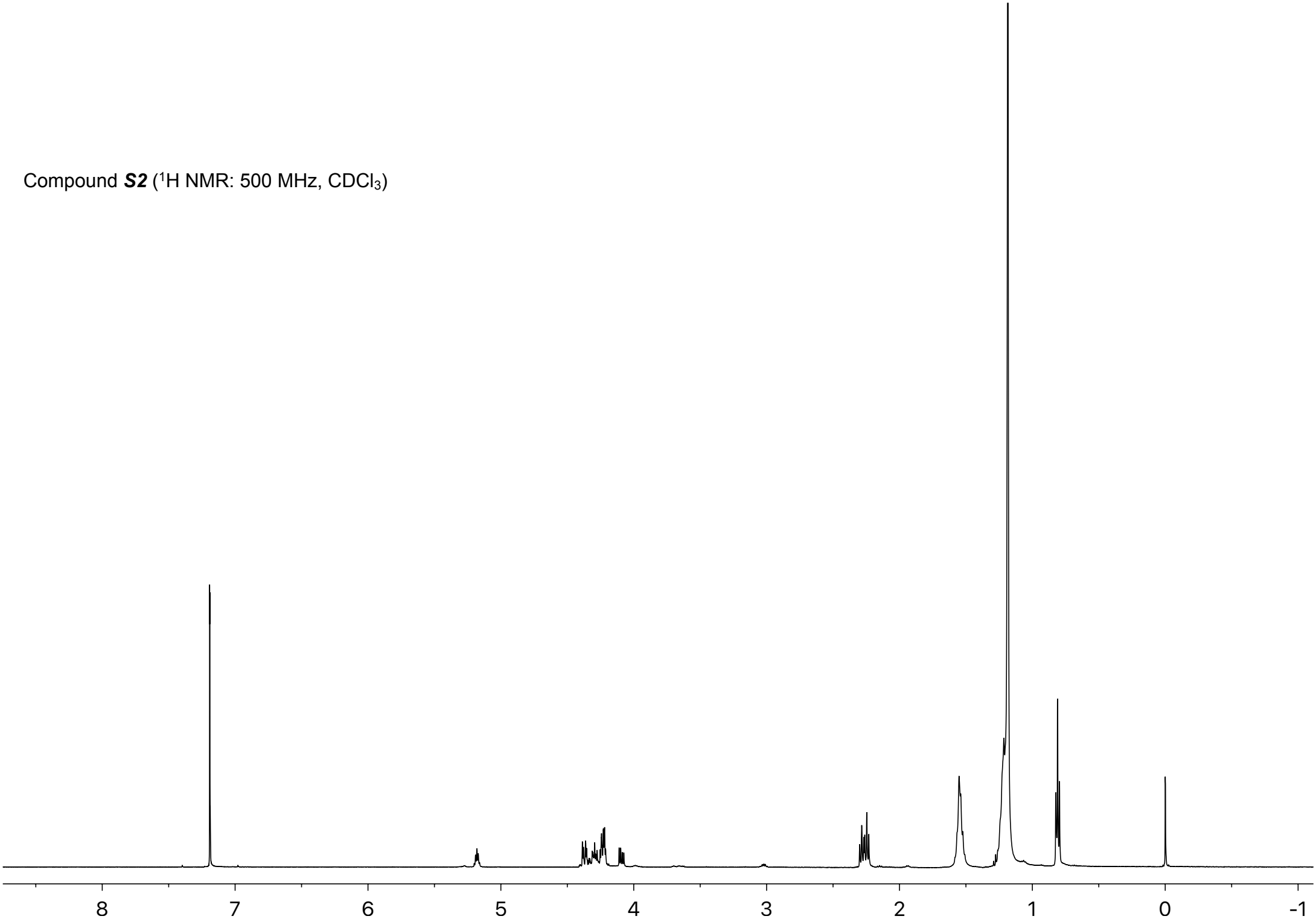

Compound ***S2*** (^{13}C NMR: 126 MHz, $CDCl_3$)

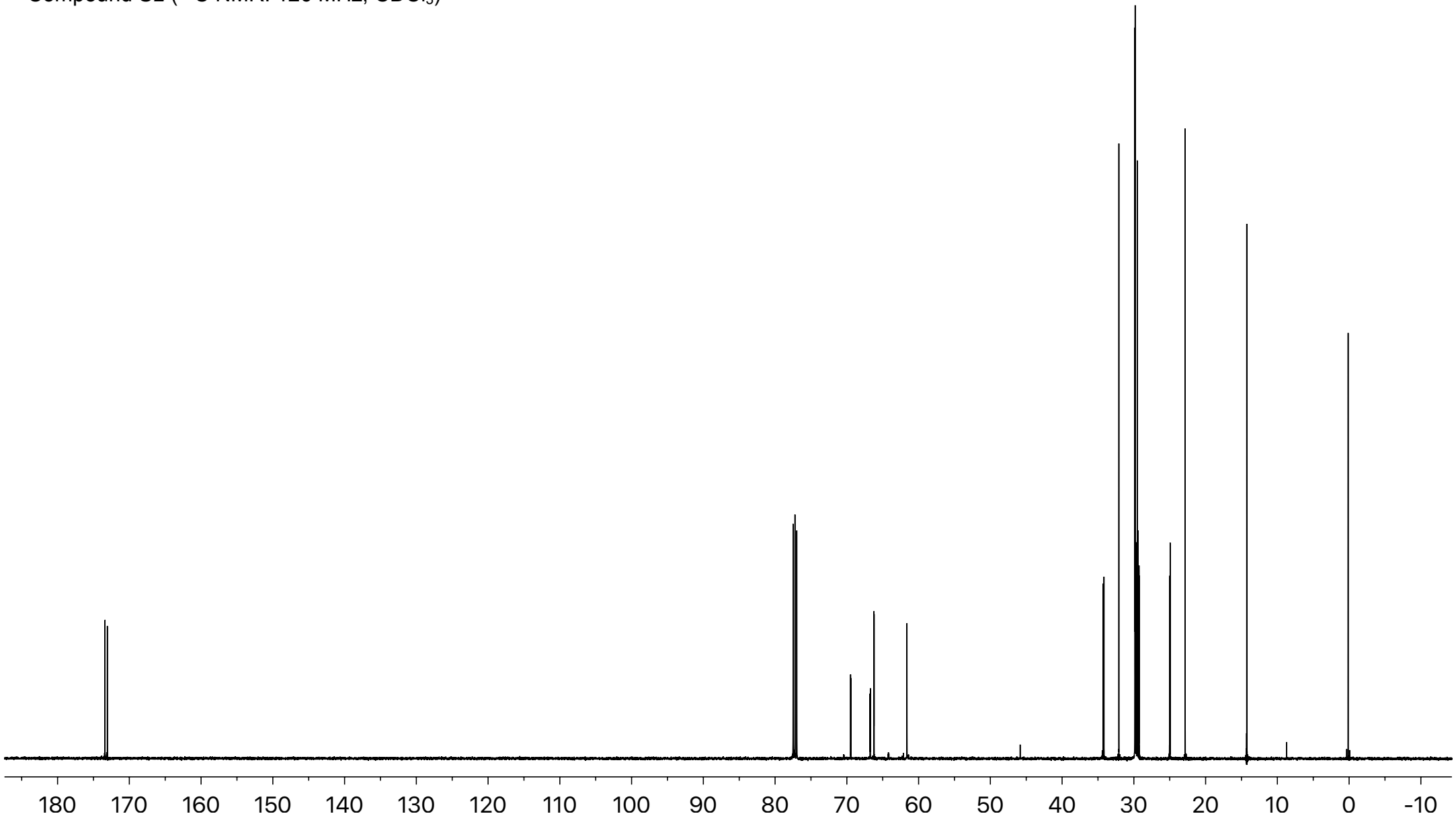

Compound ***S2*** (^{31}P NMR: 202 MHz, $CDCl_3$)

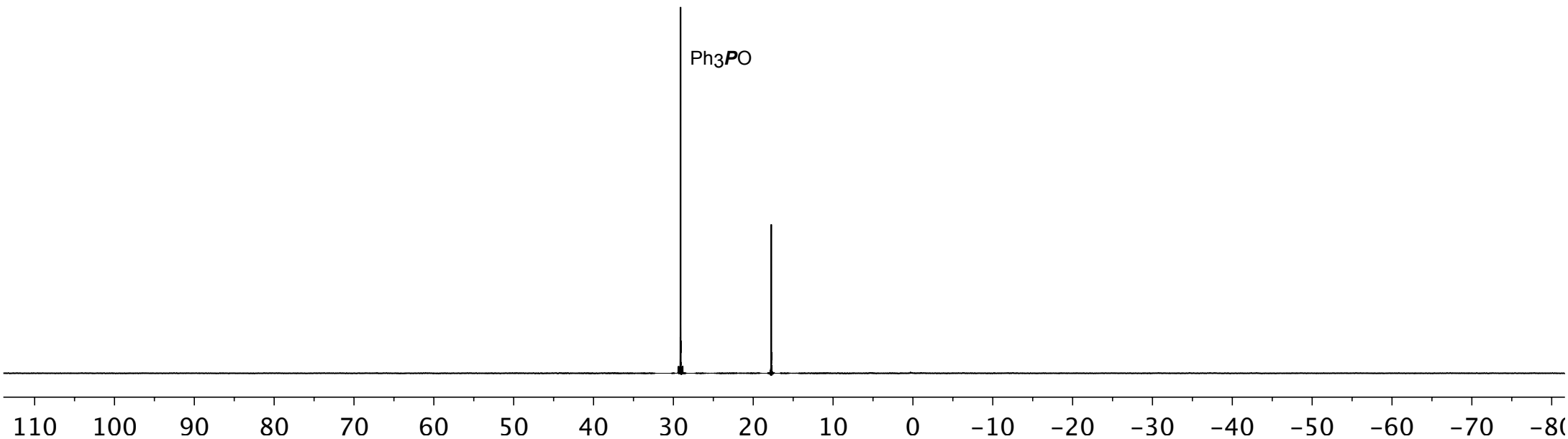

Compound ***4*** (^{1}H NMR: 500 MHz, $CDCl_3$)

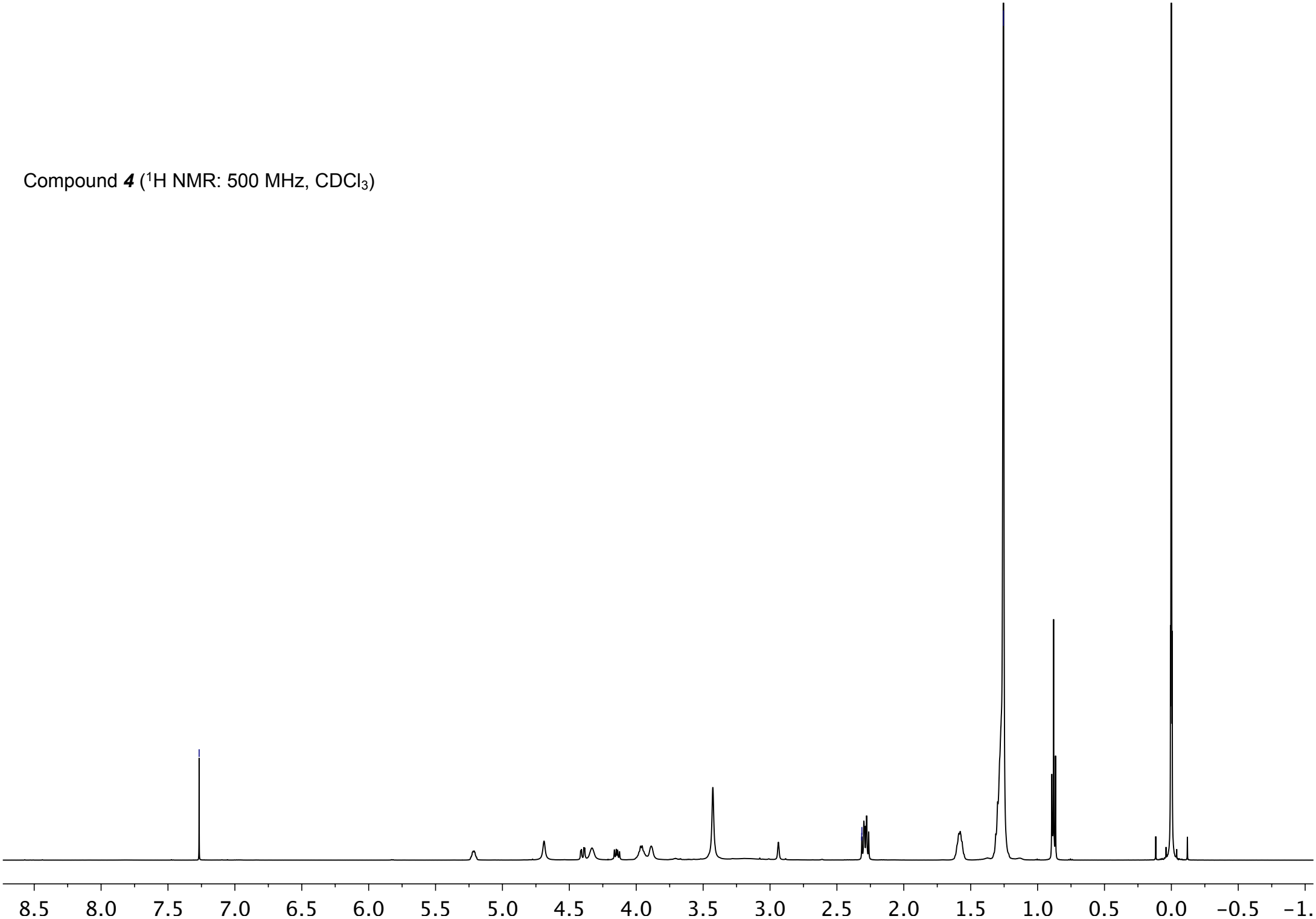

Compound ***4*** (^{13}C NMR: 126 MHz, $CDCl_3$)

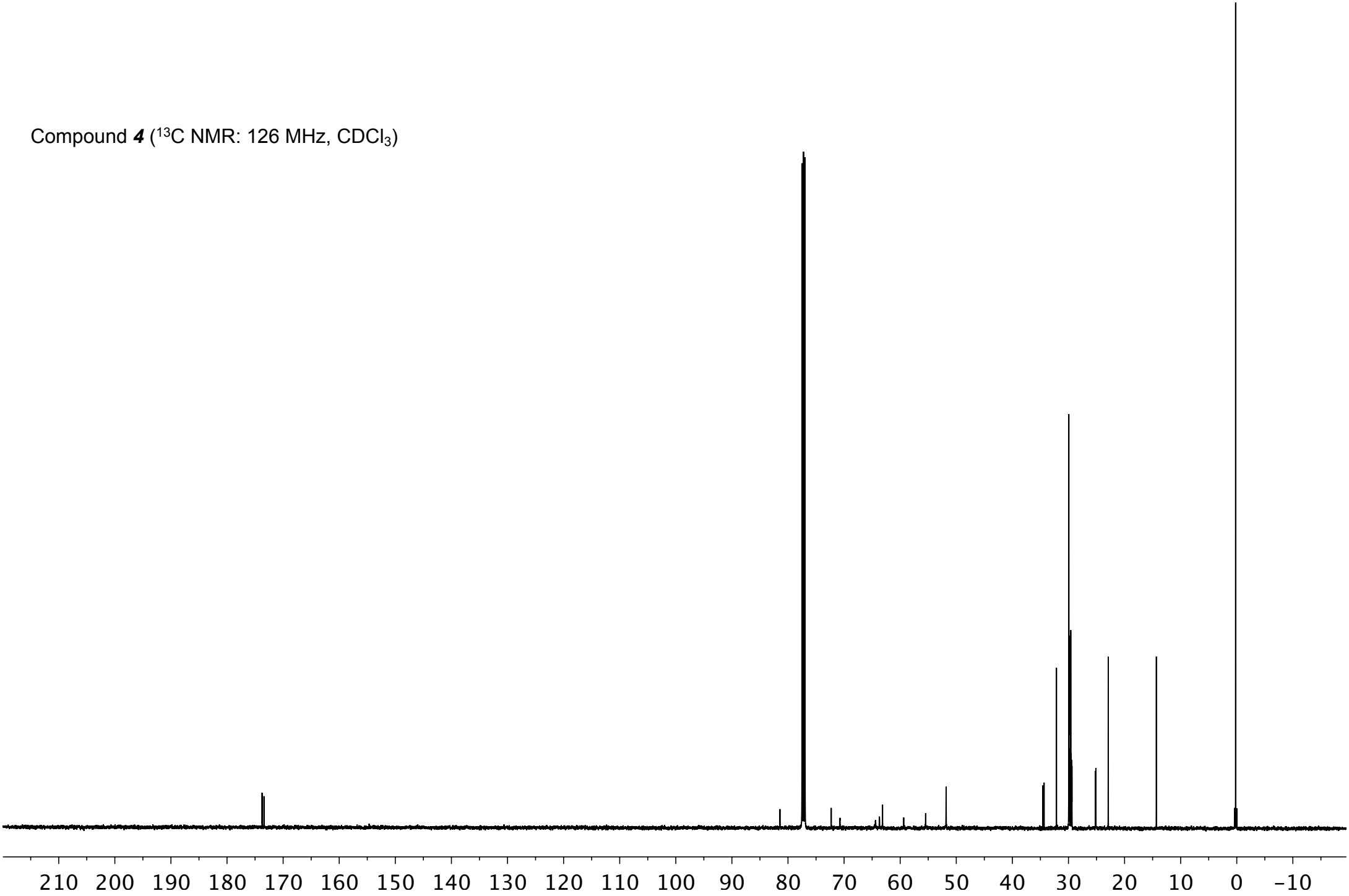

Compound ***4*** (^{31}P NMR: 202 MHz, $CDCl_3$)

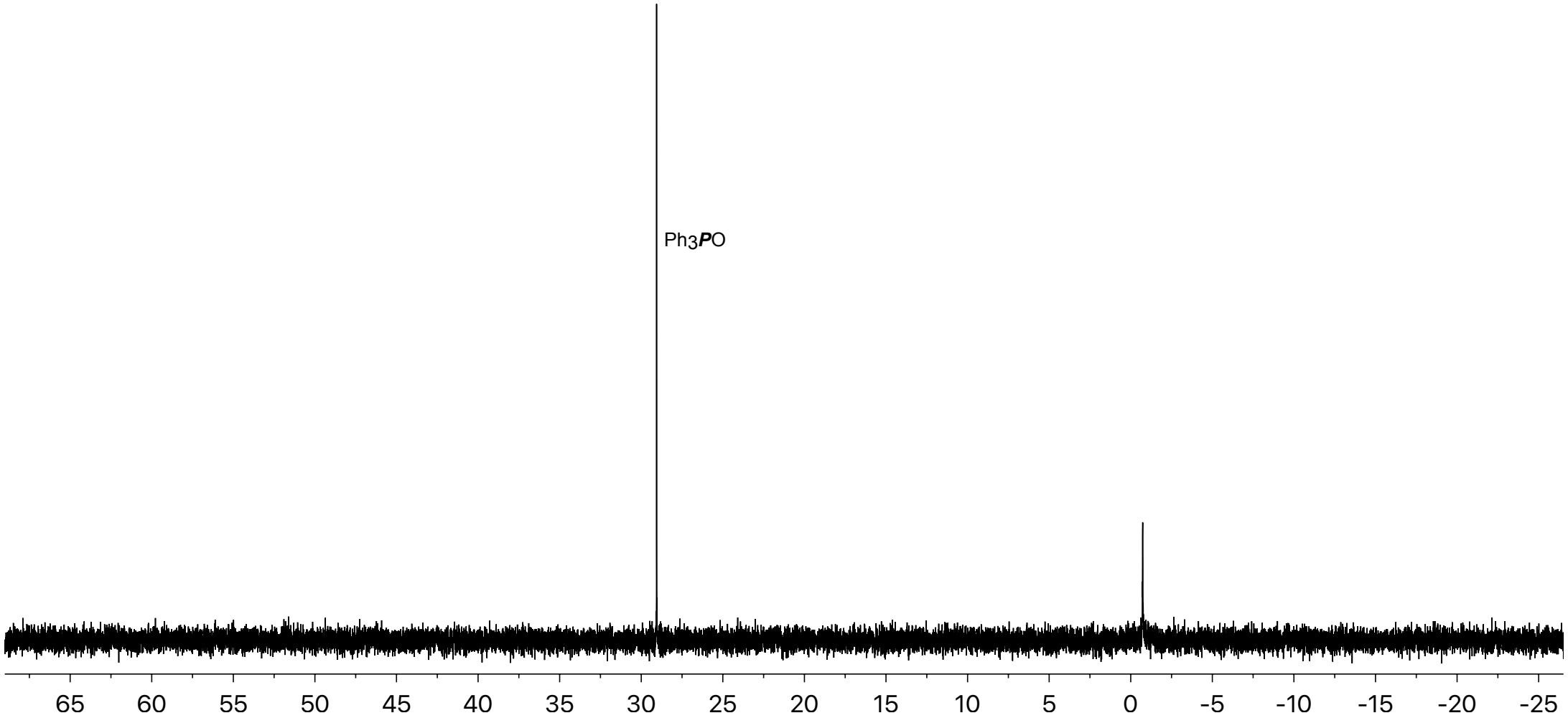

DPPC-TC-ONOO^{-} (^{1}H NMR: 500 MHz, $CDCl_3$ / CD_3OD, 3:1 v/v)

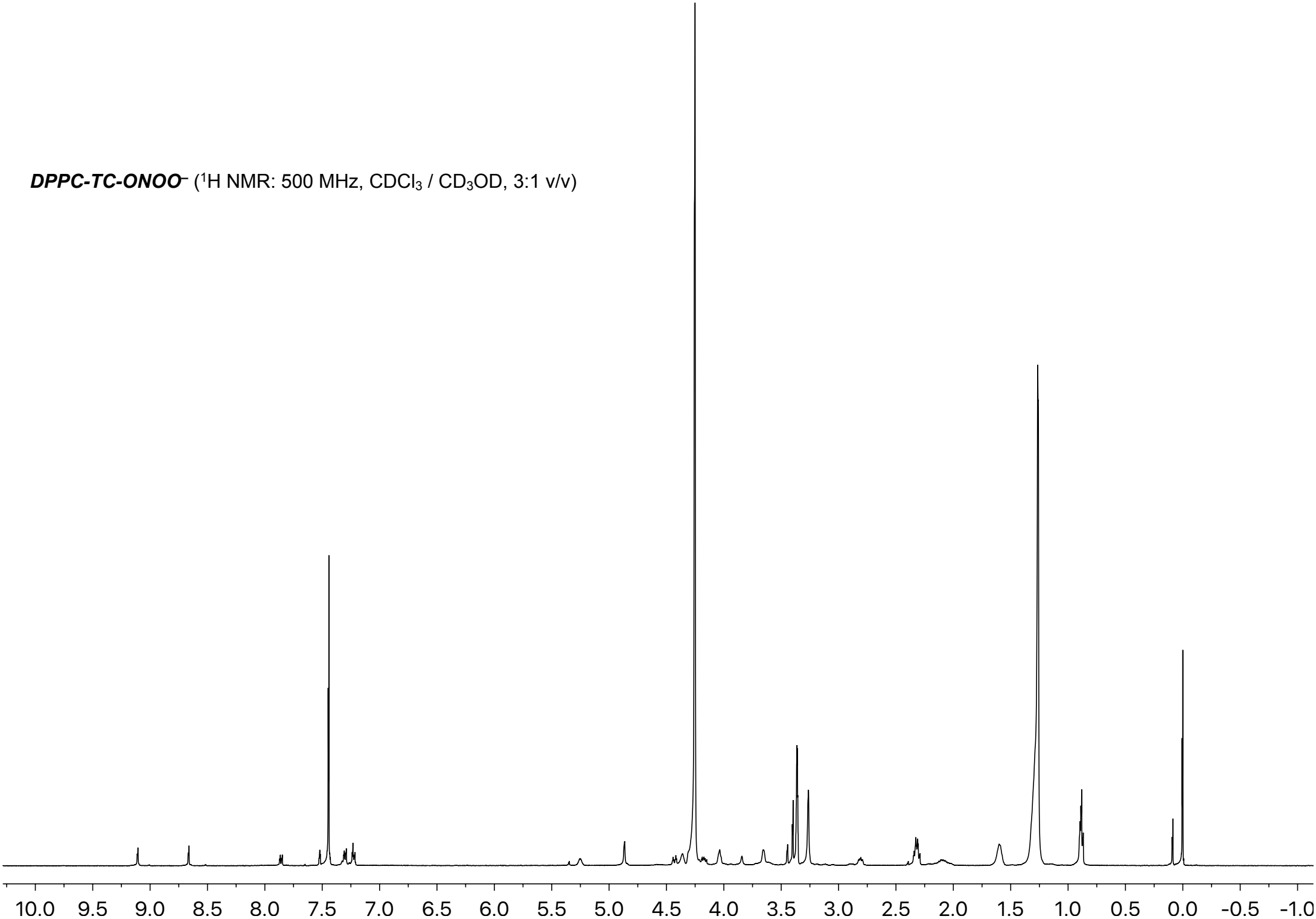

DPPC-TC-ONOO^{-} (^{13}C NMR: 126 MHz, $CDCl_3$ / CD_3OD, 3:1 v/v)

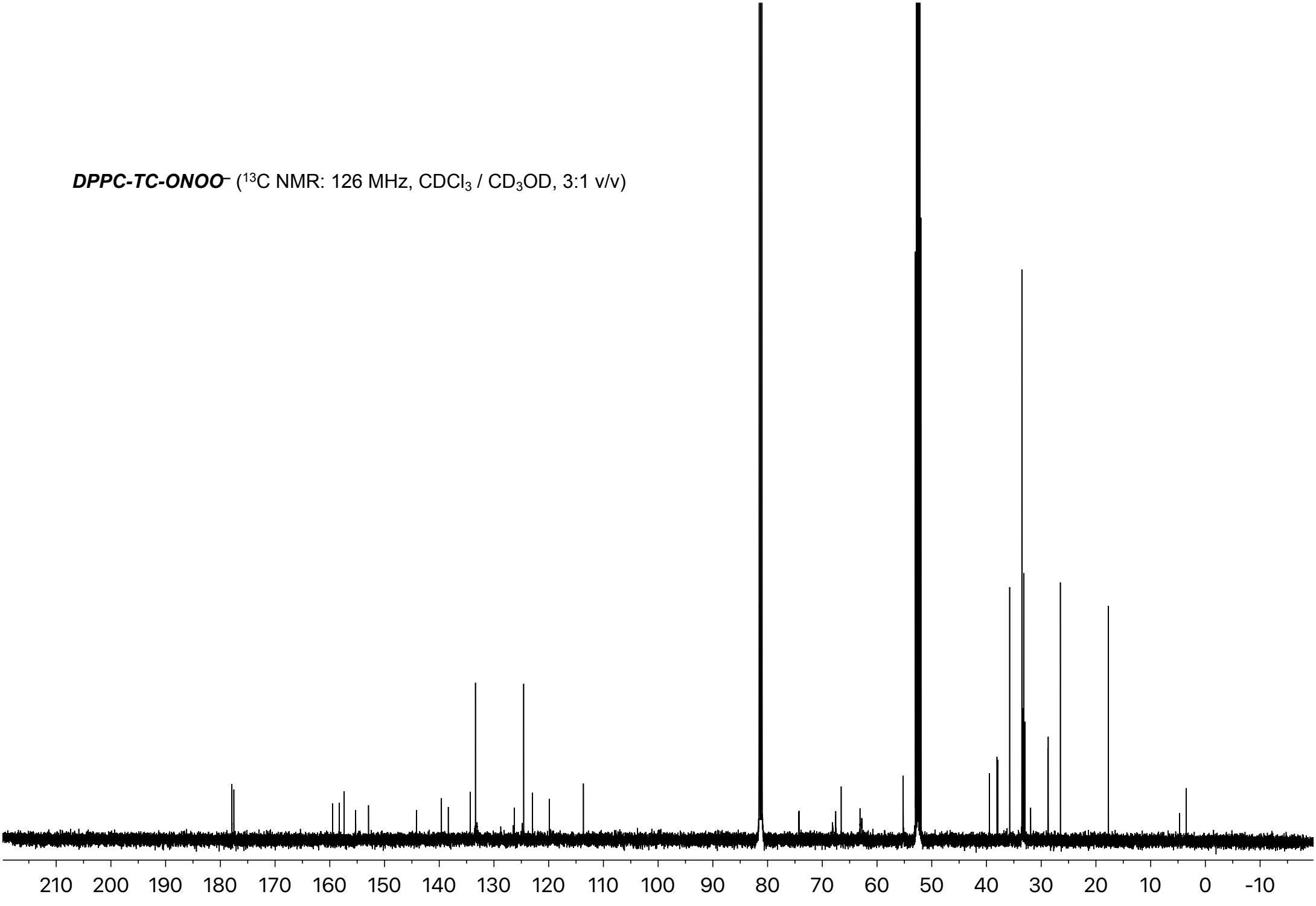

DPPC-TC-ONOO^{-} (^{31}P NMR: 202 MHz, $CDCl_3$ / CD_3OD, 3:1 v/v)

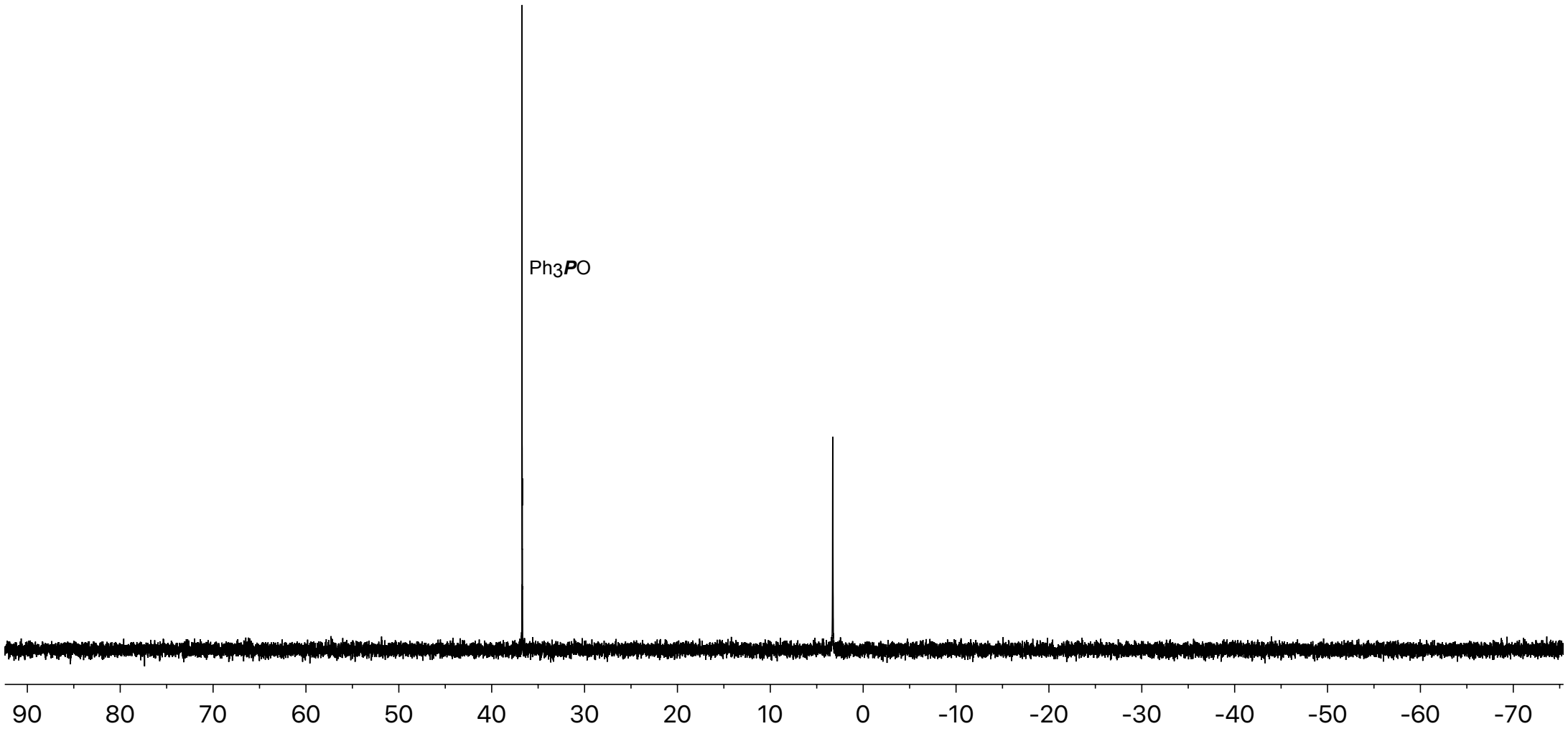

DPPC-TC-ONOO^{-} (^{19}F NMR: 471 MHz, $CDCl_3$ / CD_3OD, 3:1 v/v)

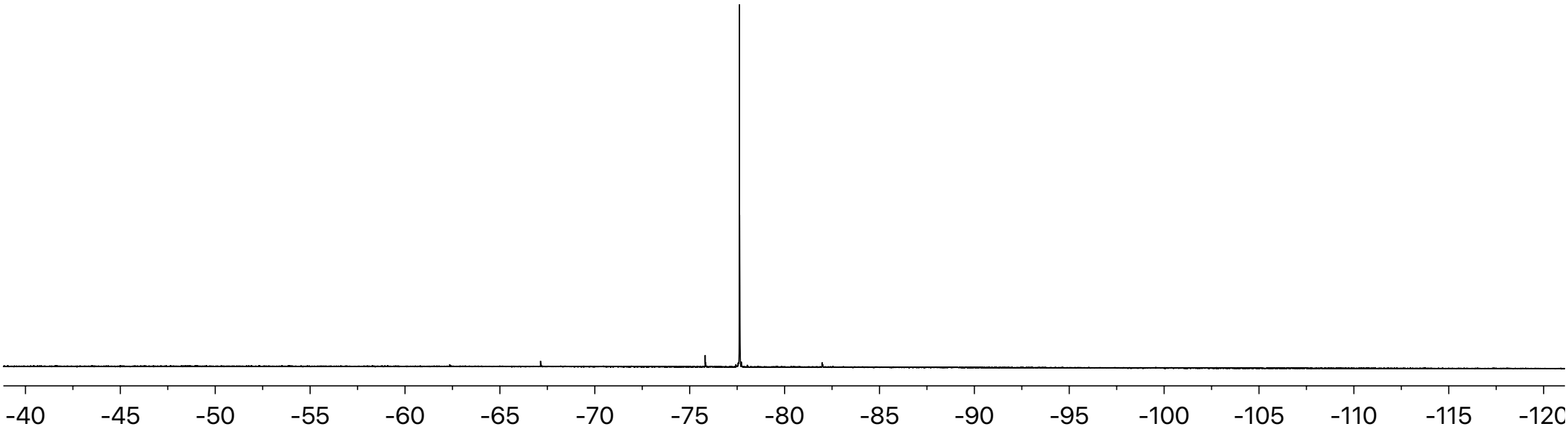

TEG-TC (^{1}H NMR: 500 MHz, CD_3OD)

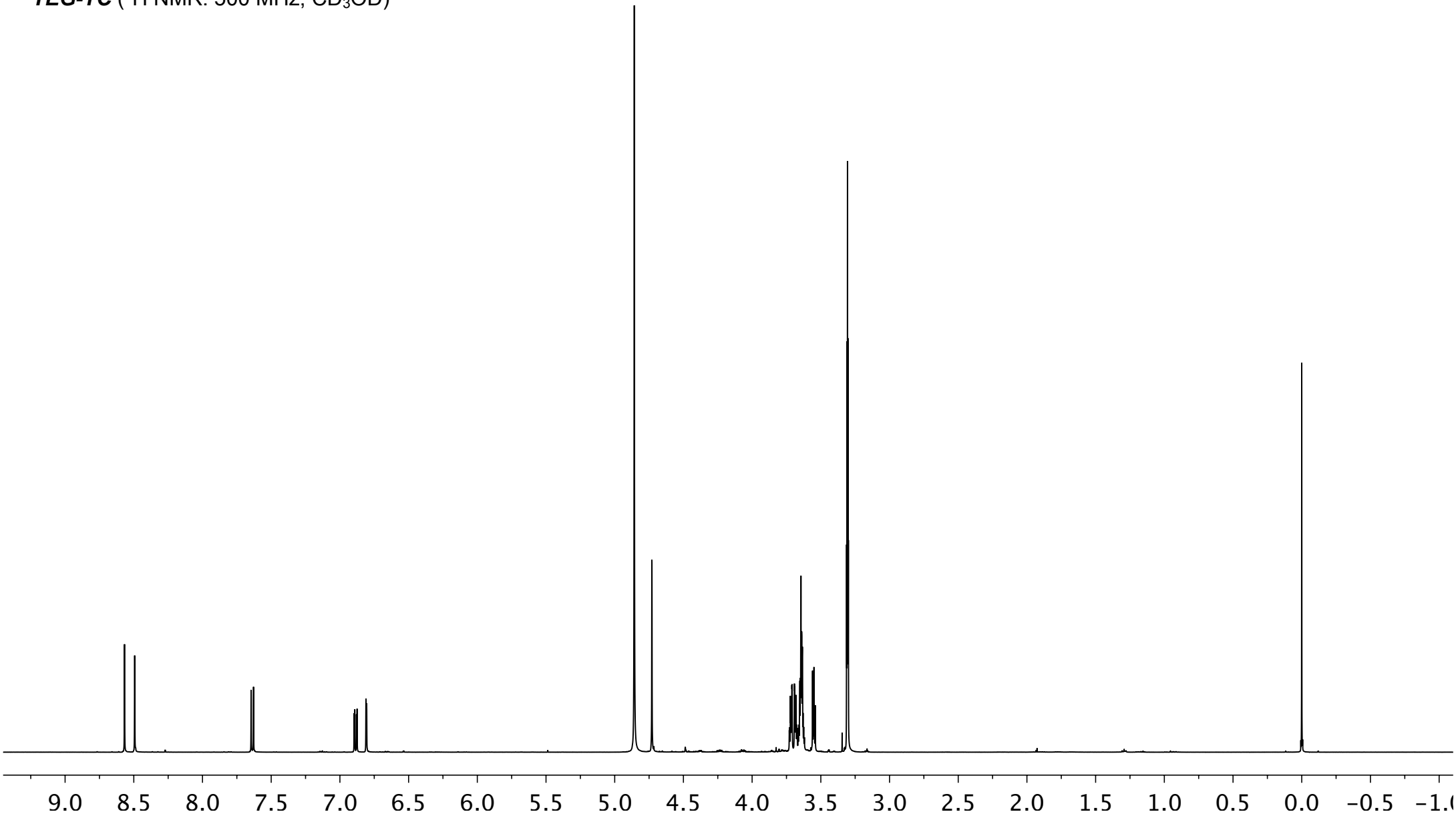

TEG-TC (^{13}C NMR: 126 MHz, CD_3OD)

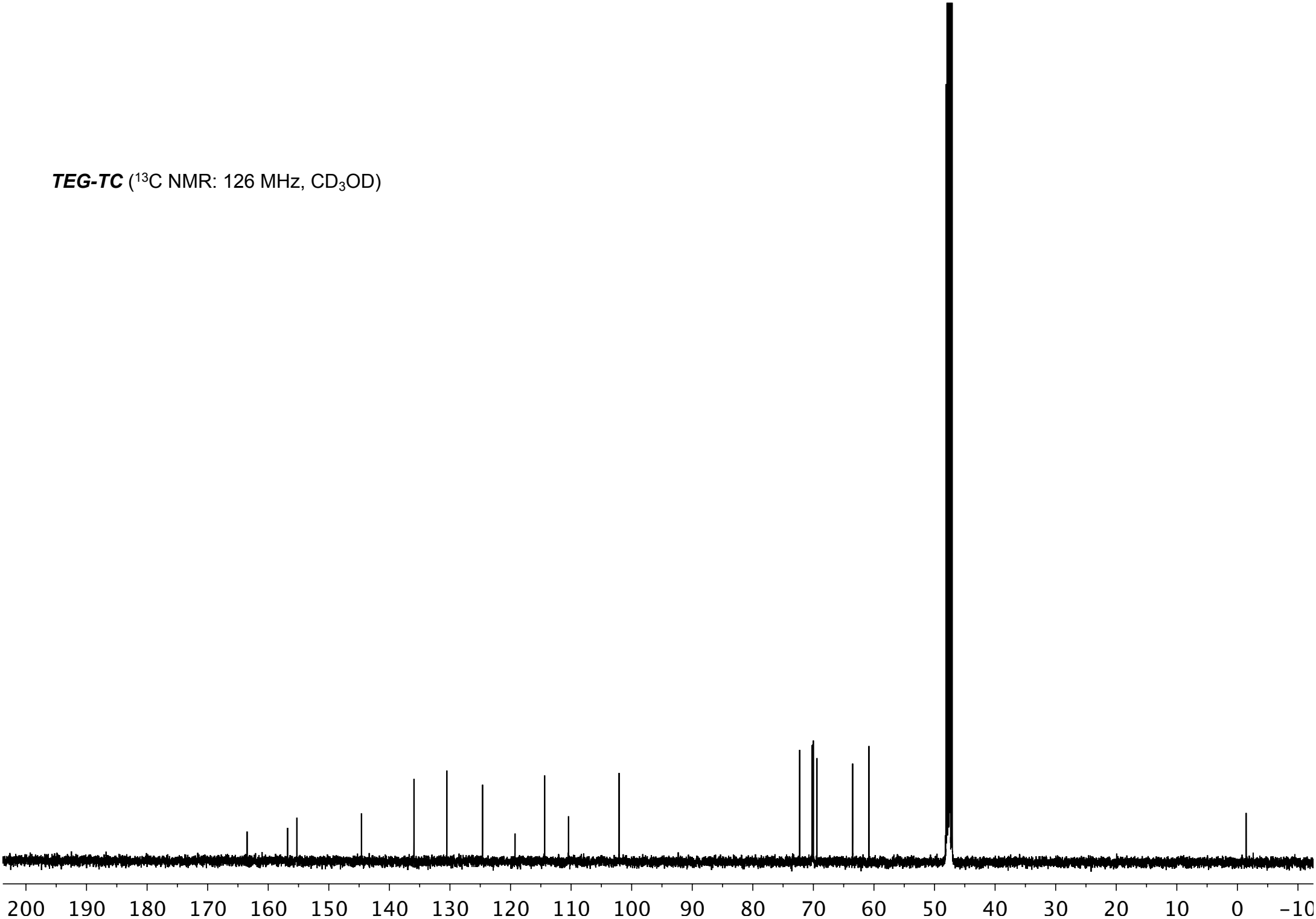

DPPC-TC (^{1}H NMR: 500 MHz, $CDCl_3$ / CD_3OD, 3:1 v/v)

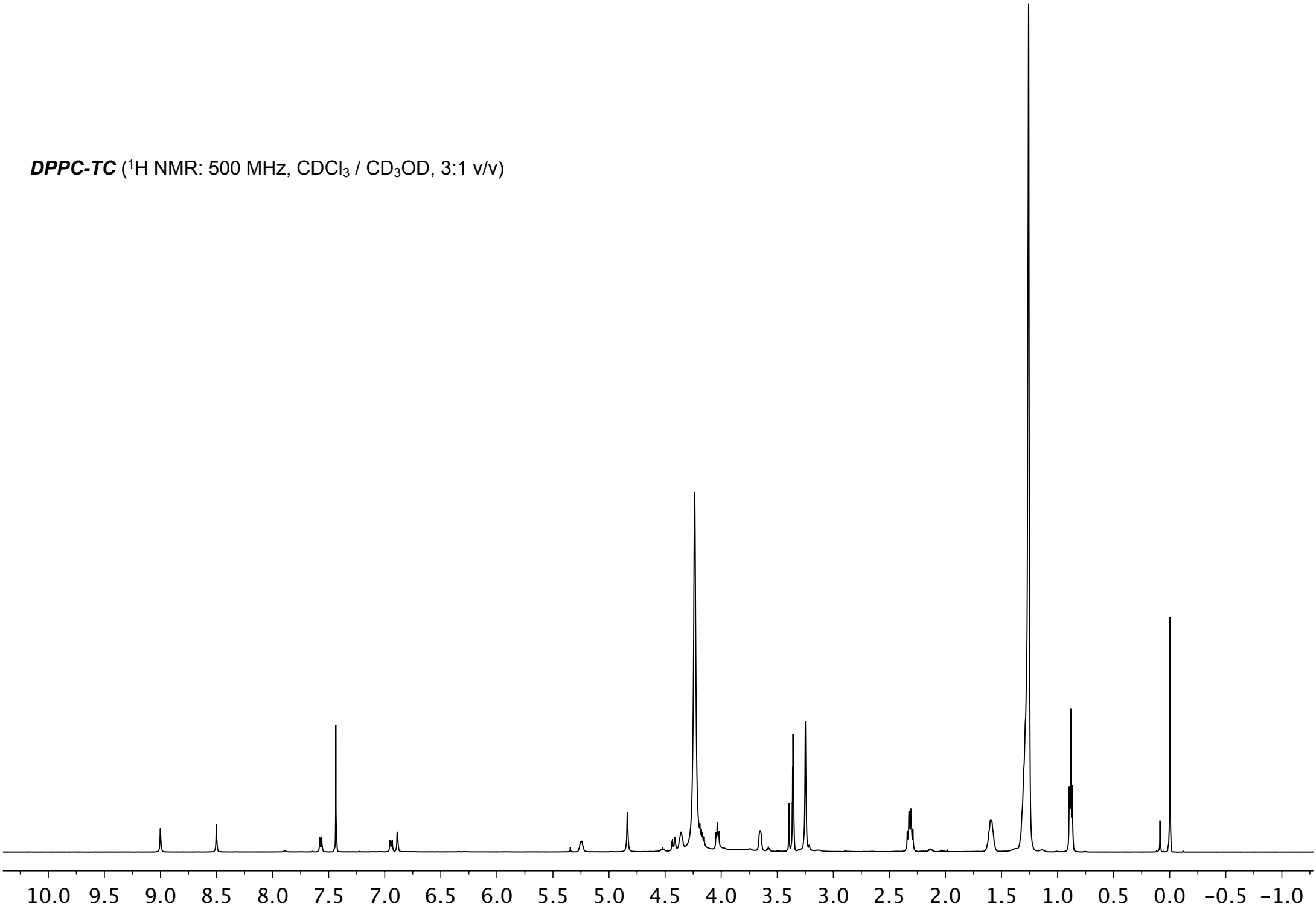

DPPC-TC (^{13}C NMR: 126 MHz, $CDCl_3$ / CD_3OD, 3:1 v/v)

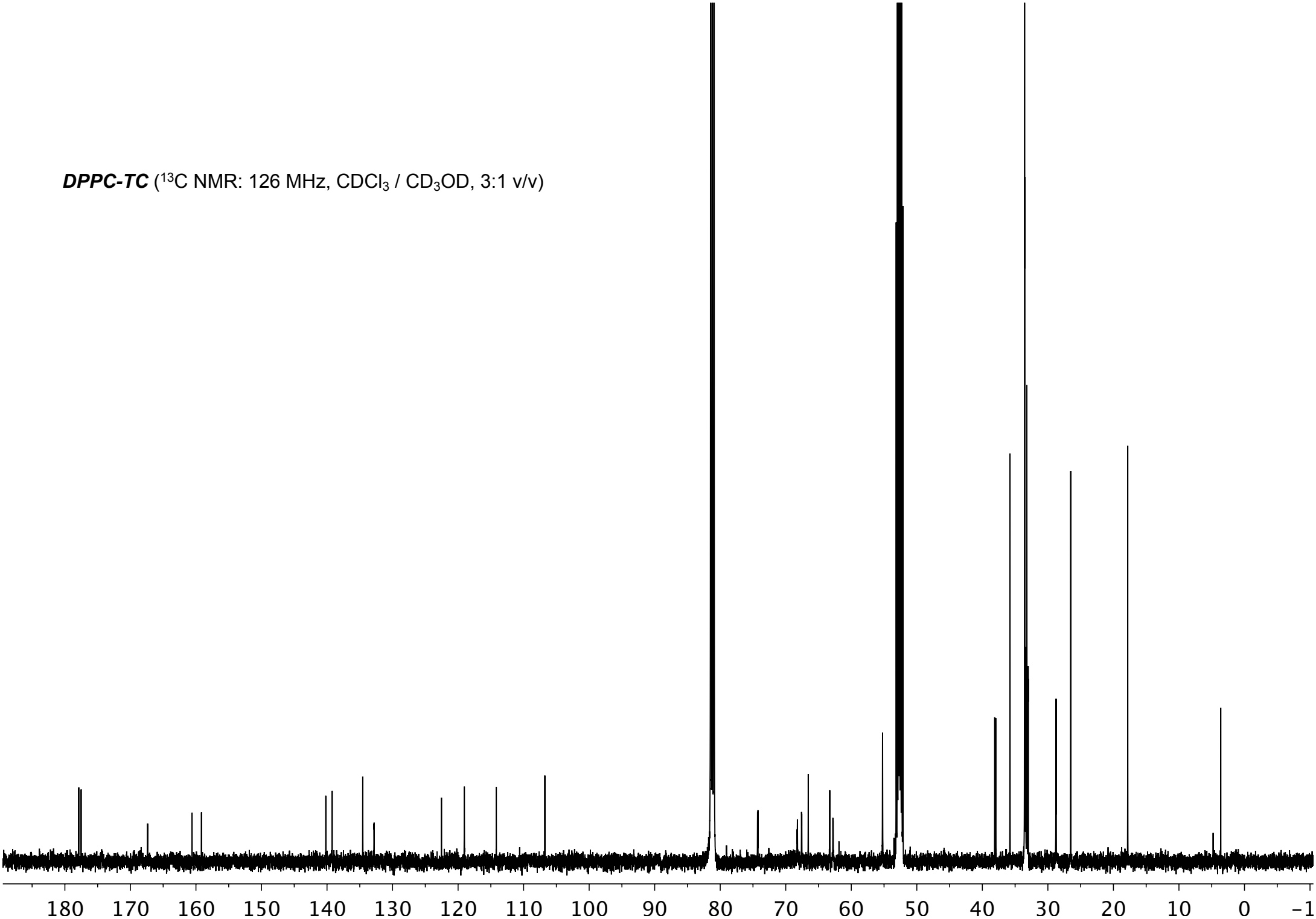

DPPC-TC (^{31}P NMR: 202 MHz, $CDCl_3$ / CD_3OD, 3:1 v/v)

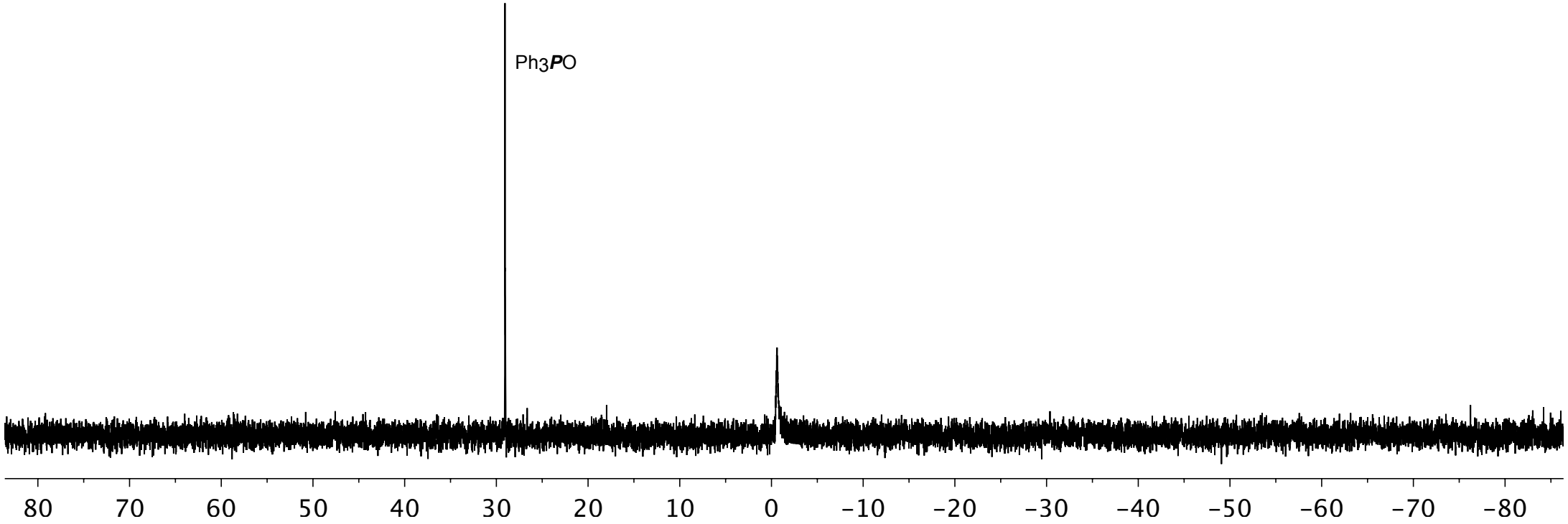

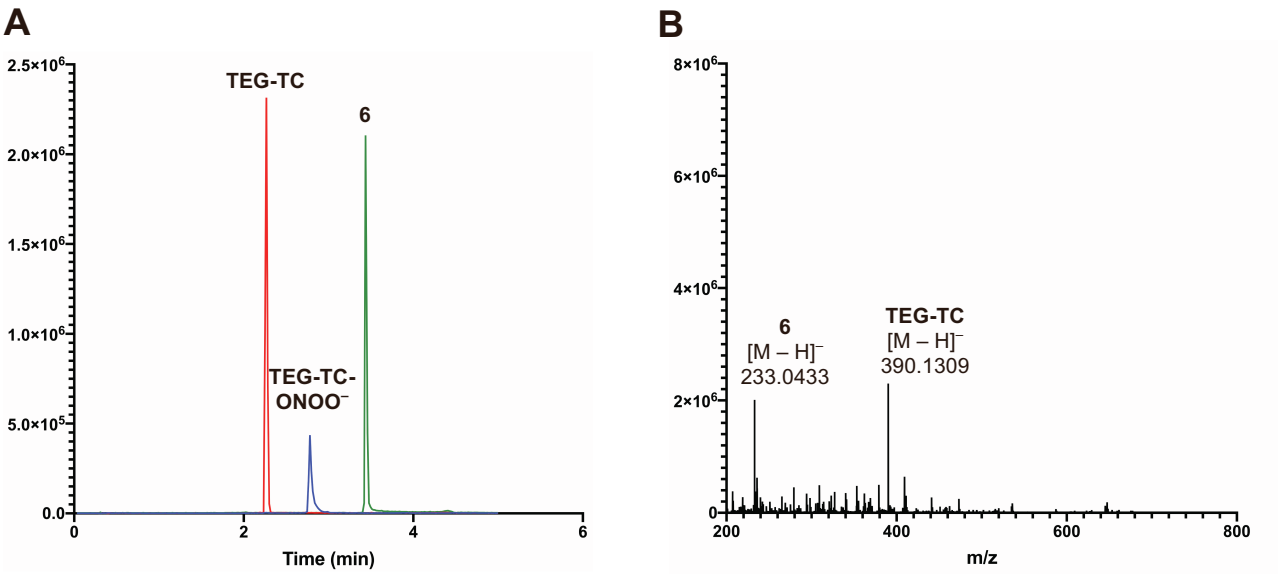

Figure S1. LCMS analysis of reaction of TEG-TC-ONOO⁻ with ONOO⁻, related to Figure 1.

(A) Overlay of extracted ion chromatograms of compounds **TEG-TC** (red), **TEG-TC-ONOO⁻** (blue), and the oxa-spiro[4,5] decenone **6** (green) as the major products from the reaction (5 minutes) between **TEG-TC-ONOO⁻** (10 μM) and $ONOO^-$ (600 μM). Reaction solvent: H_2O/MeOH (1:4 v/v). Aqueous part contained Tris (50 mM, pH 7.5). **(B)** HRMS analysis of the reaction aliquot taken in 5 minutes. Spectra are shown for the retention times of 2–4 minute window. HRMS analysis was carried out in negative ionization mode. **TEG-TC: HRMS** (ESI) m/z: Calculated for $C_{18}H_{20}N_3O_7^-$, [M - H]⁻, requires 390.1307; found 390.1309. The oxa-spiro[4,5] decenone **6: HRMS** (ESI) m/z: Calculated for $C_{10}H_8F_3O_3^-$, [M – H] ⁻, requires 233.0431; found 233.0433.

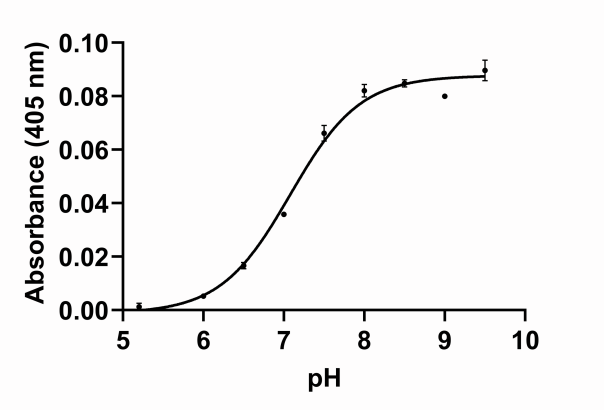

Figure S2. Determination of pK_a of TEG-TC, related to Figure 1.

Absorbance (405 nm) of **TEG-TC** vs. pH. For each absorbance measurement, a 20 μM solution of **TEG-TC** was prepared in buffers with different pH values: 5.2, 6.0, 7.0, 7.5, 8.0, 8.5, 9.0, and 9.5. The buffers at pH 5.2 and 6.0 were obtained using 50 mM MES, while those at pH 7.0–9.5 were obtained using 50 mM Tris. Resulting data was fitted to a sigmoidal curve, providing a pK_a of 7.1 ± 0.1 (R^2 = 0.989). Error bars represent standard deviation, n = 3.

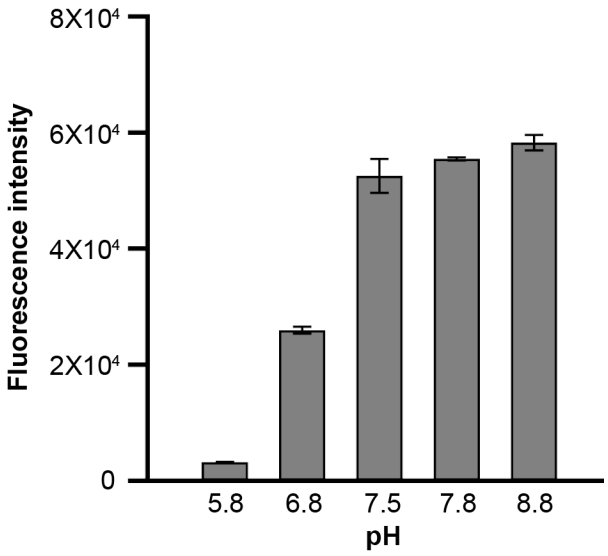

Figure S3. The pH dependence of fluorescence intensity for TEG-TC, related to Figures 1 and 2

The fluorescence intensity (405 nm excitation, 475 nm emission) of the model coumarin **TEG-TC** (1 μM) was measured in buffer solutions with pH values: 5.8, 6.8, 7.5, 7.8, and 8.8. The buffer at pH 5.8 was obtained using 50 mM MES, while those at pH 6.8–8.8 were obtained using 50 mM Tris. Error bars represent standard deviation, *n* = 3.

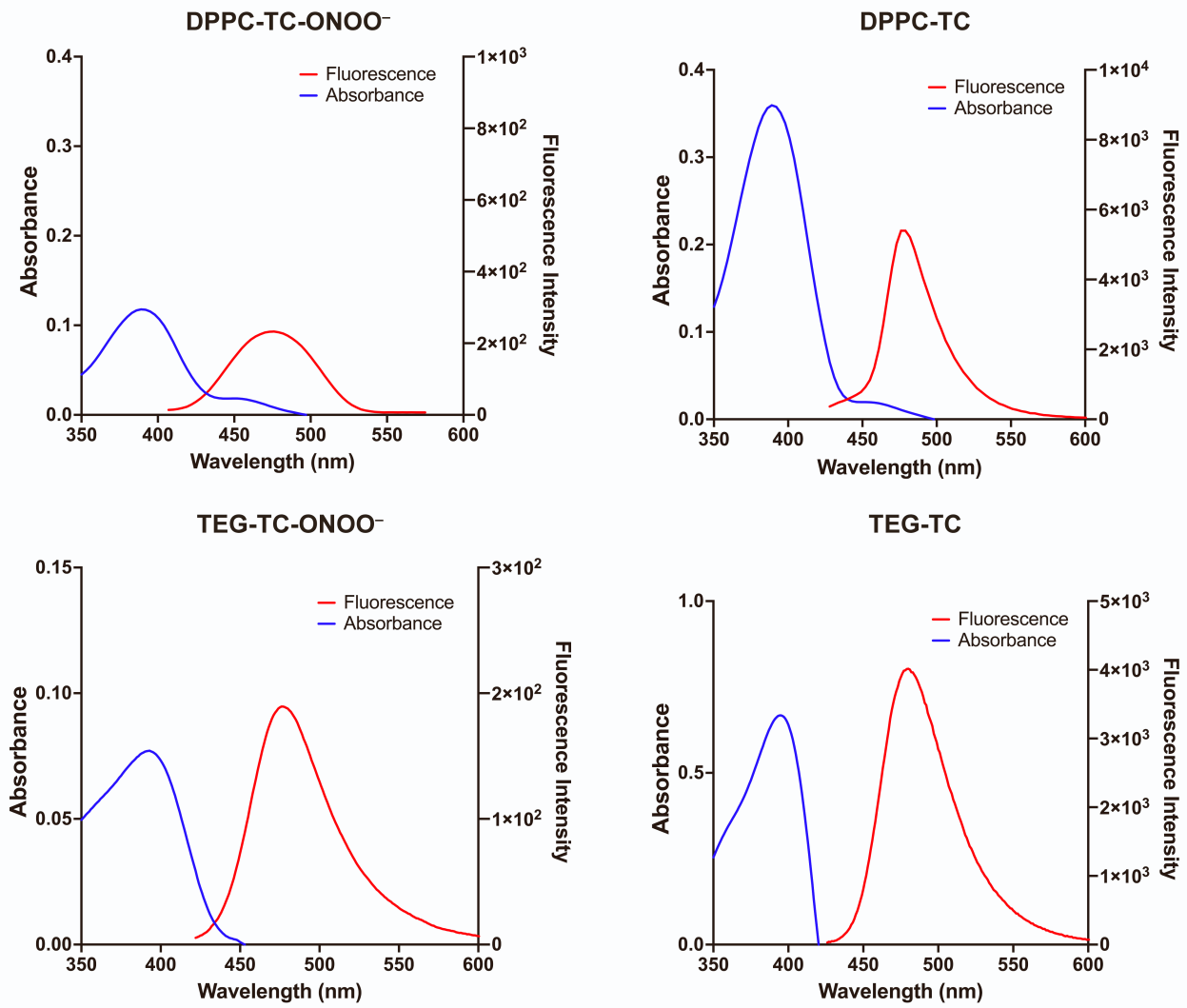

Figure S4. Spectrophotometric characterizations by absorbance and emission, related to Figures 1 and 2

Absorbance and emission profiles of the probes and their uncaged analogs.

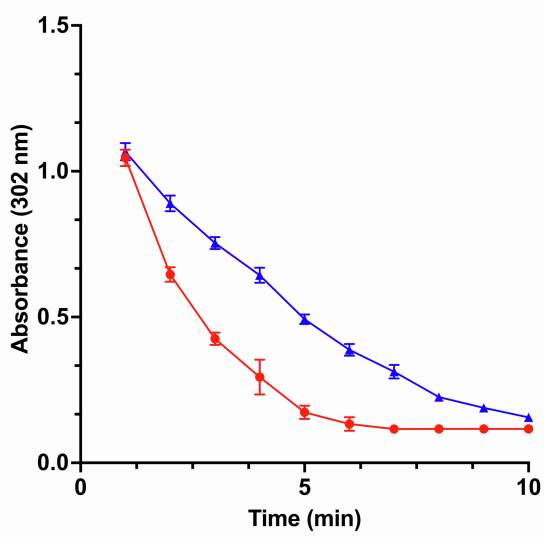

Figure S5. UV-Vis spectrophotometric investigation of peroxynitrite, related to Figure 2

Two sets of data were acquired based on CO_2 treatment: (1) CO_2-rich and (2) CO_2-deprived. (1) For the CO_2-rich condition, the peroxynitrite-free aqueous buffer was first bubbled with CO_2 gas from dry ice and the pH was adjusted to 7.5 by careful addition of NaOH. (2) For the CO_2-deprived condition, the peroxynitrite-free aqueous buffer was first boiled to eliminate CO_2, and the pH was adjusted to 7.5 by careful addition of HCl. A freshly prepared $ONOO^-$ solution (2.2 mM, pH 10.6) was added to each buffer and the absorbance at 302 nm was recorded over 10 minutes. Based on dilution, the concentration of $ONOO^-$ at the moment of mixing was estimated to be 600 μM. Error bars represent standard deviation, n = 3. Variation in pH after addition of $ONOO^-$ was undetermined.

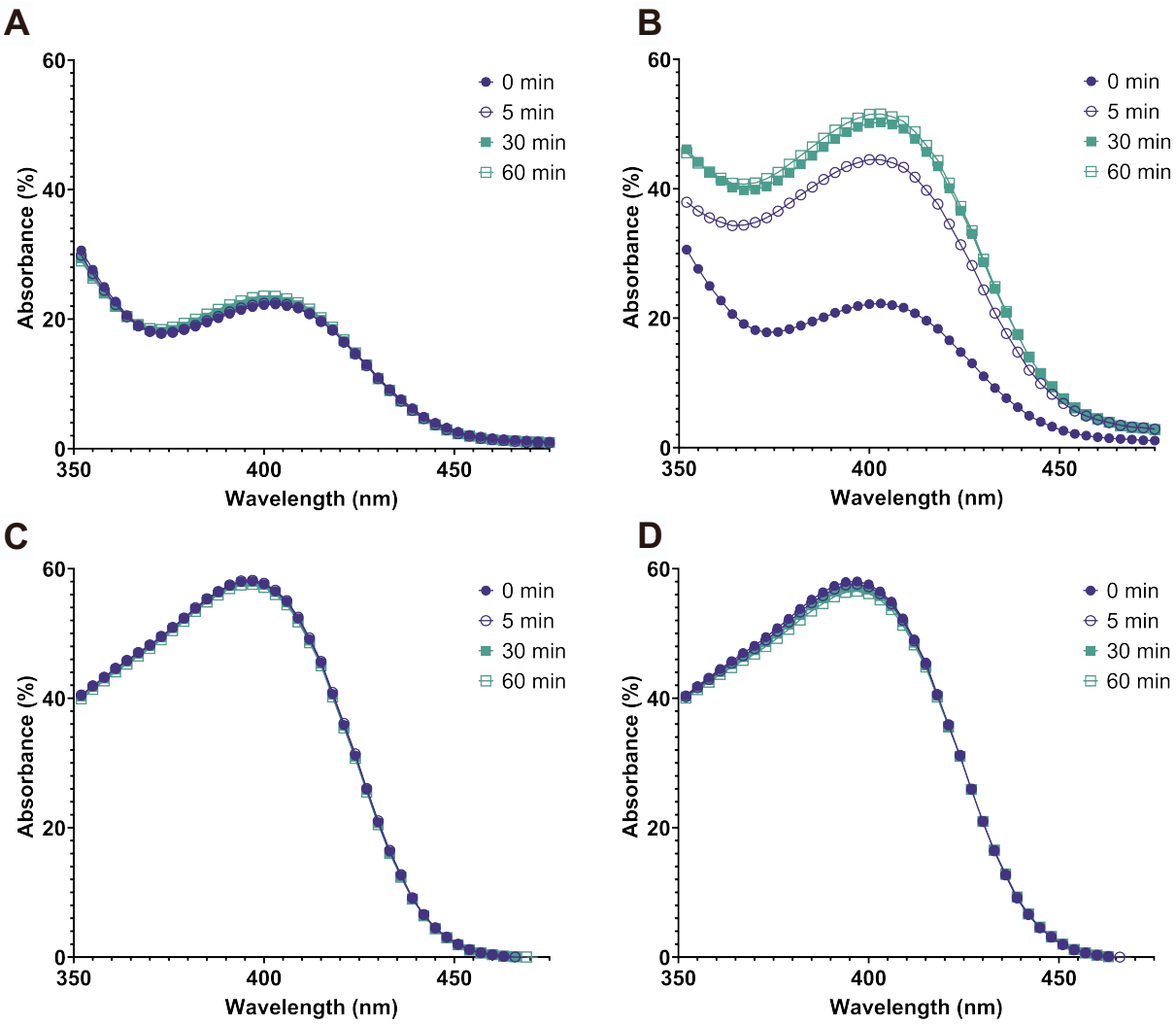

Figure S6. Effect of peroxynitrite on TEG-TC-ONOO$^-$, related to Figure 2.

Time course for the UV-Vis absorbance of the aqueous mixtures including **(A) TEG-TC-ONOO$^-$** (200 μM), **(B) TEG-TC-ONOO$^-$** (200 μM) and peroxynitrite (600 μM), **(C) TEG-TC** (200 μM), and **(D) TEG-TC** (200 μM) and peroxynitrite (600 μM). Percent conversion of the probe **TEG-TC-ONOO$^-$** into the coumarin **TEG-TC** by peroxynitrite was 67% at 5 minutes and 88% at 60 minutes. All mixtures were prepared in Tris buffer (150 mM, pH 7.5). Data acquired at room temperature. Blank included Tris buffer and DMSO. Probe **TEG-TC-ONOO$^-$** and the coumarin **TEG-TC** were initially dissolved in DMSO, then introduced into the buffer.

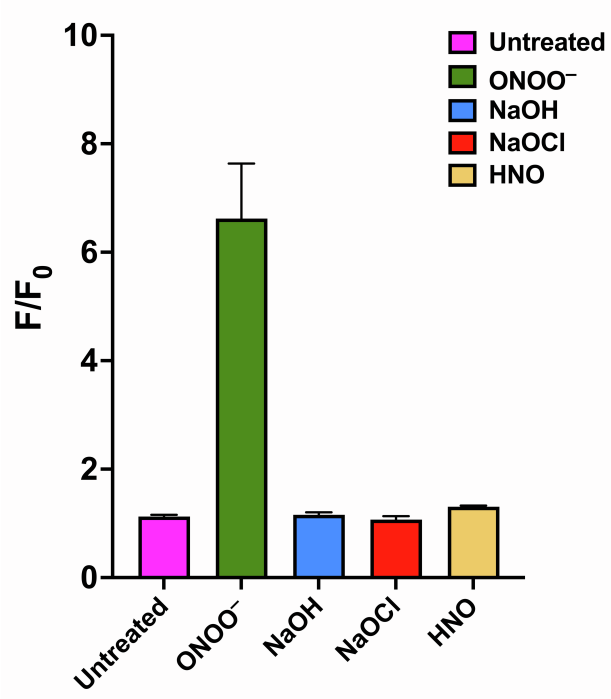

Figure S7. Additional redox selectivity measurements, related to Figure 2

Selectivity of **TEG-TC-ONOO**$^-$ against HO^-, ClO^-, and HNO. **TEG-TC-ONOO**$^-$ (1 μM) was dissolved in Tris buffer (50 mM, pH 7.5) and subjected to the redox species with an estimated initial concentration of 600 μM. Data represent F/F0 measurements of samples incubated for 60 min. F and F0 are defined as the fluorescence with and without the redox agent. Ex/Em: 405/475 nm. Error bars represent standard deviation, n = 3.

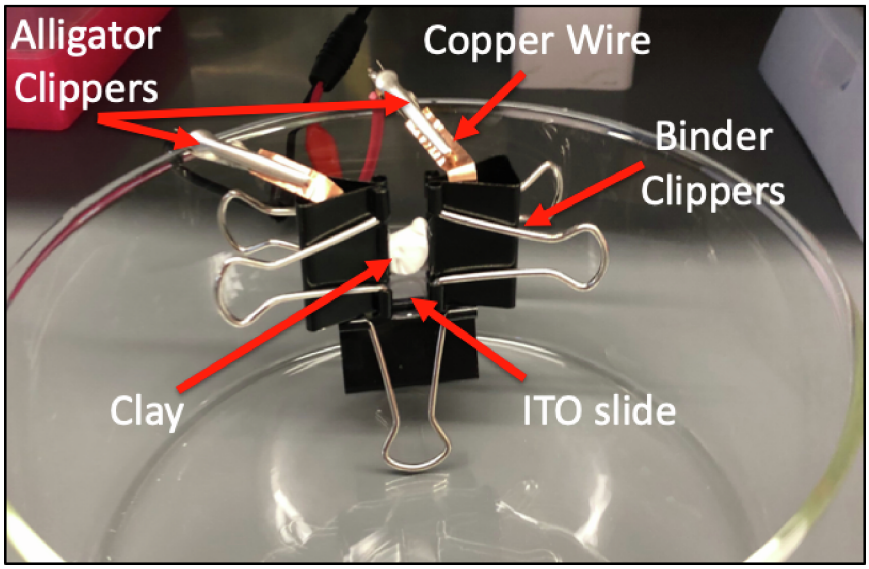

Figure S8. Preparation of giant vesicles, related to Figure 3

The electroformation chamber used to form GVs.

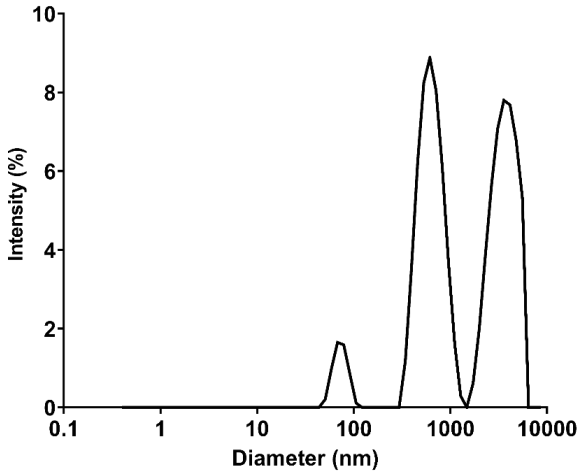

Figure S9. DLS analysis of giant vesicles, related to Figure 3

DLS analysis of the vesicles prepared via electroformation. Approximately 48% of the vesicles had an average size of 5 μm in diameter.

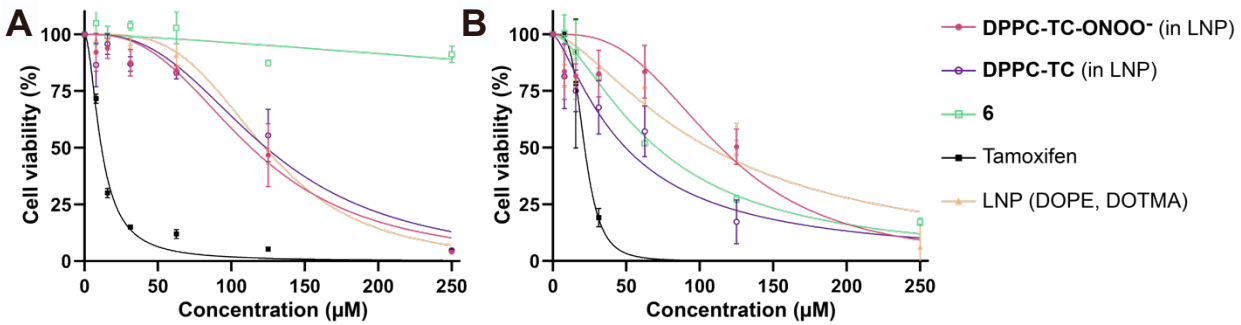

Figure S10. Determination of cytotoxicity, related to Figures 4 and 5

MTT assay for **(A)** HeLa and **(B)** RAW 264.7 cells after 24 hours of treatment. For each OD_{570} value, the % cell viability vs. concentration plots were obtained using GraphPad Prism 8 software. Error bars represent standard error of mean, *n* = 3.

Table S1. Summary of IC_{50} for HeLa (rows 1-2) and RAW 264.7 (rows 3-4), related to Figures 4 and 5

	IC_{50} (μM) with 95% CI				
	DPPC-TC-ONOO⁻	**DPPC-TC**	**6**	**Tamoxifen**	**LNP (DOPE, DOTMA)**
HeLa	113 ± 14	124 ± 18	>250[a]	12 ± 1	123 ± 6
RAW 264.7	114 ± 28	49 ± 13	71 ± 8	22 ± 2	106 ± 28

[a] Compound displayed no detectable level of cytotoxicity at 250 μM, which constitutes for the upper bound IC_{50} value. CI: Confidence interval.

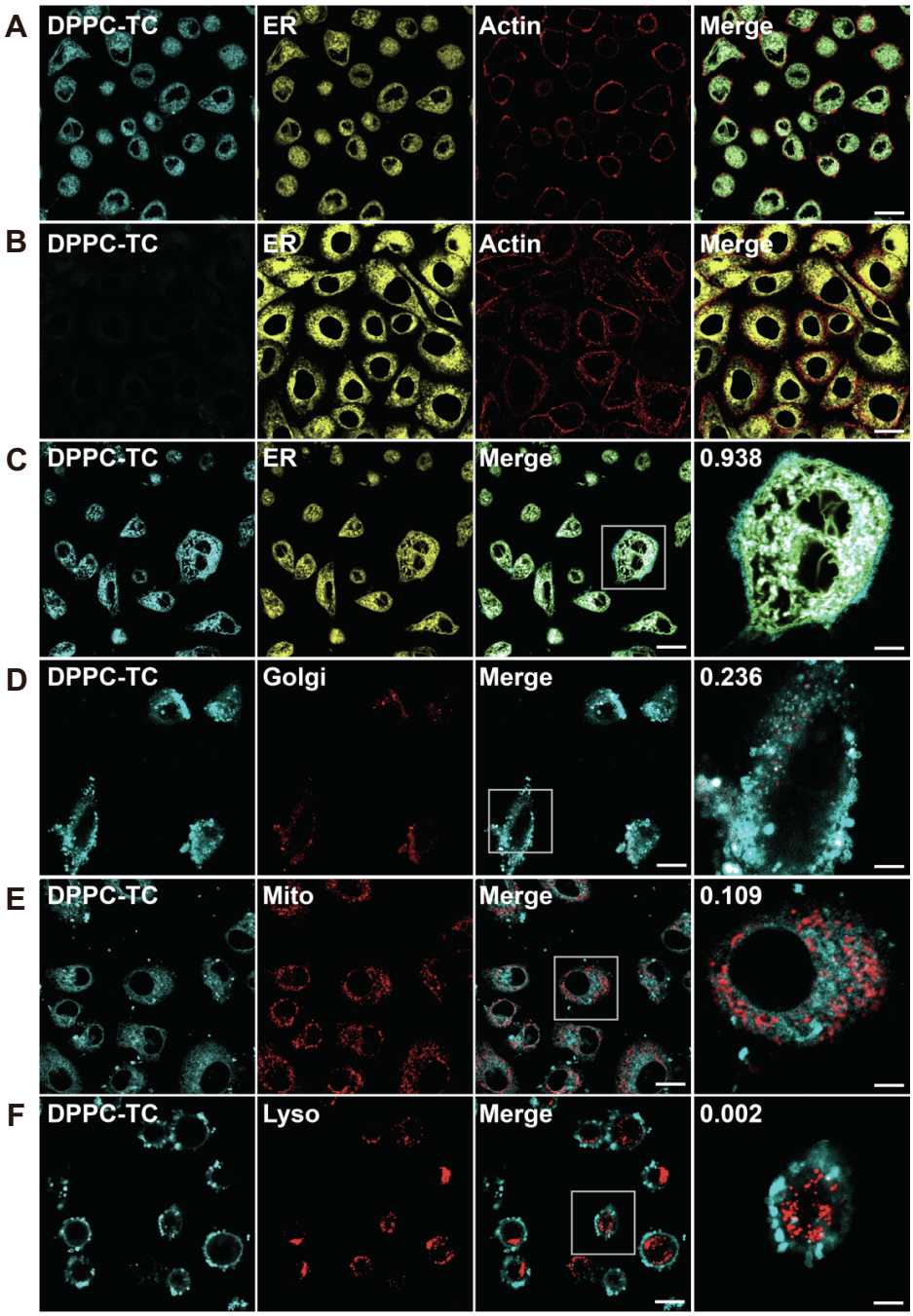

Figure S11. Confocal imaging of lipid environments targeted by $ONOO^-$ in live HeLa, related to Figure 4

LNPs obtained from a 47.5 : 47.5 : 5.0 molar ratio of DOTMA, DOPE, and **(A) DPPC-TC** or **(B–F) DPPC-TC-$ONOO^-$**. **(A-B)** Cells treated with LNPs, left unstimulated. **(C–F)** Quantitative colocalization study of cells treated with LNPs and stimulated with IFN-γ/LPS/PMA. PCC was calculated for assessment of colocalization. DPPC-TC channel: 405/475 nm. Scale bars = 20 μm or 5 μm (zoomed area).

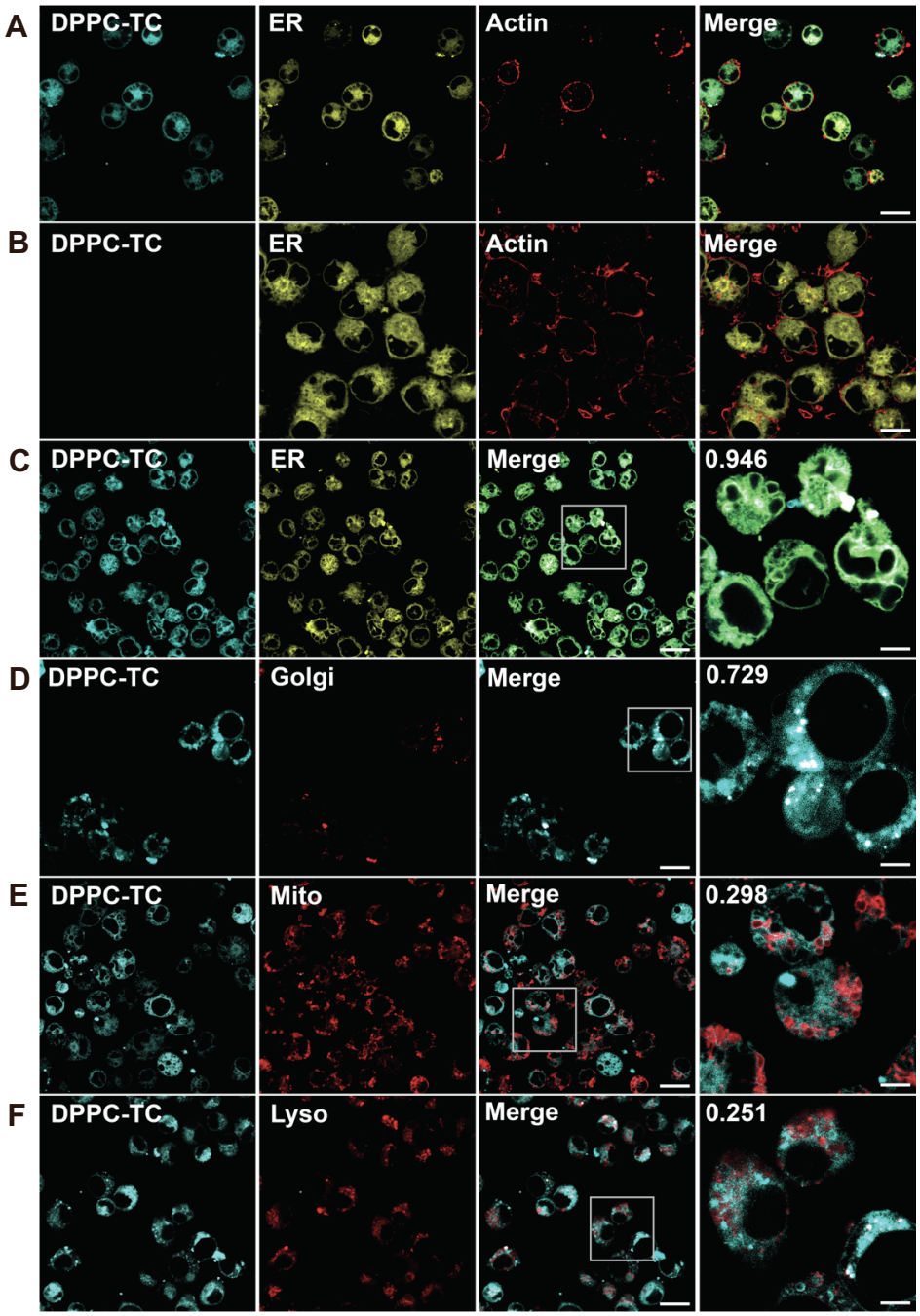

Figure S12. Confocal imaging of lipid environments targeted by $ONOO^-$ in live RAW 264.7 cells, related to Figure 5

LNPs obtained from a 47.5 : 47.5 : 5.0 molar ratio of DOTMA, DOPE, and **(A) DPPC-TC** or **(B–F) DPPC-TC-$ONOO^-$**. **(A-B)** Cells treated with LNPs, left unstimulated. **(C–F)** Quantitative colocalization study of cells treated with LNPs and stimulated with LPS. PCC was calculated for assessment of colocalization. DPPC-TC channel: 405/475 nm. Scale bars = 20 μm or 5 μm (zoomed area).

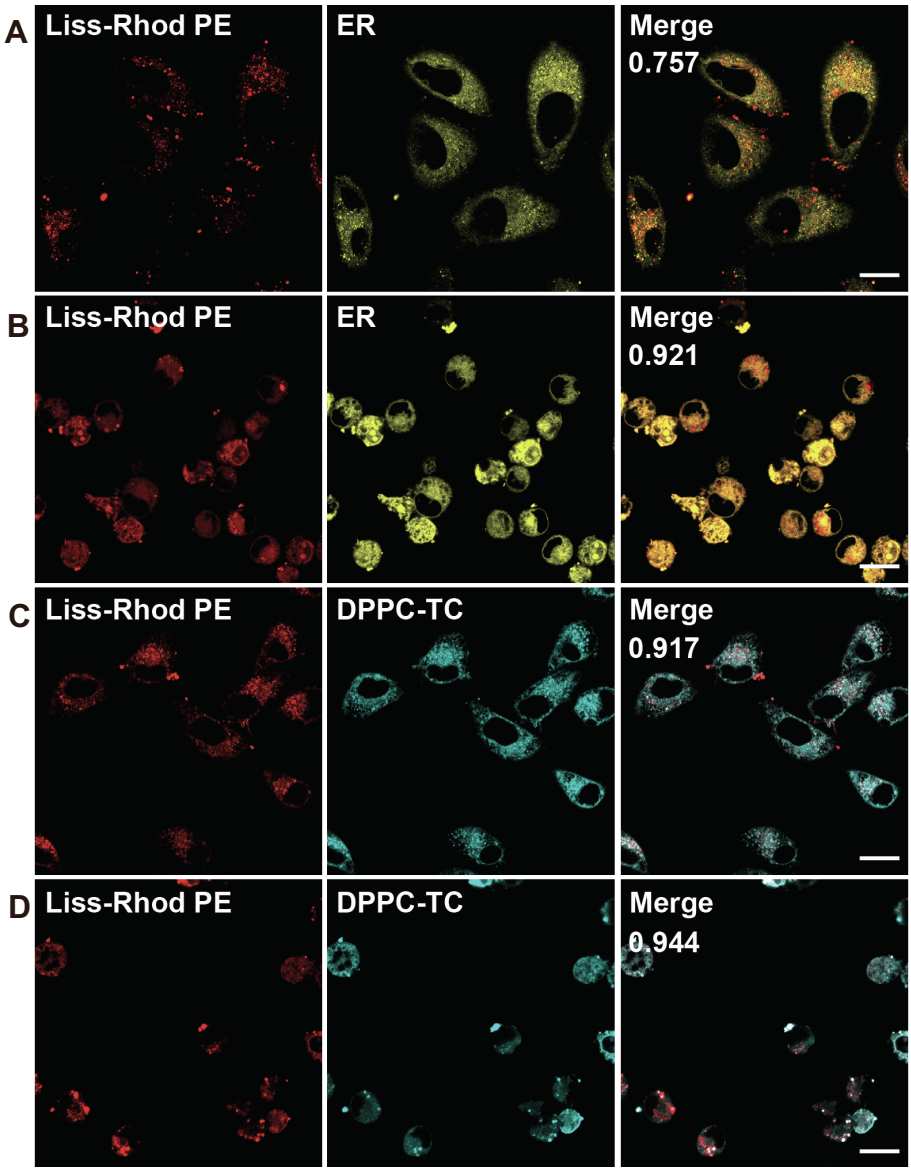

Figure S13. Confocal images of live cells using LNPs with Liss-Rhod PE, related to Figures 4 and 5

Confocal images of HeLa **(A, C)** and RAW 246.7 **(B, D)** cells incubated with LNPs containing Liss-Rhod PE and then endogenously stimulated to generate $ONOO^-$. **(A, B)** Cells were labeled with ER tracker. LNPs included a mixture of Liss-Rhod PE / DOPE / DOTMA at a 0.5 : 49.75 : 49.75 molar ratio. **(C, D)** LNPs included a mixture of Liss-Rhod PE / **DPPC-TC-$ONOO^-$** / DOPE / DOTMA at a 0.5 : 4.5 : 47.5 : 47.5 molar ratio. Scale bars = 20 μm.

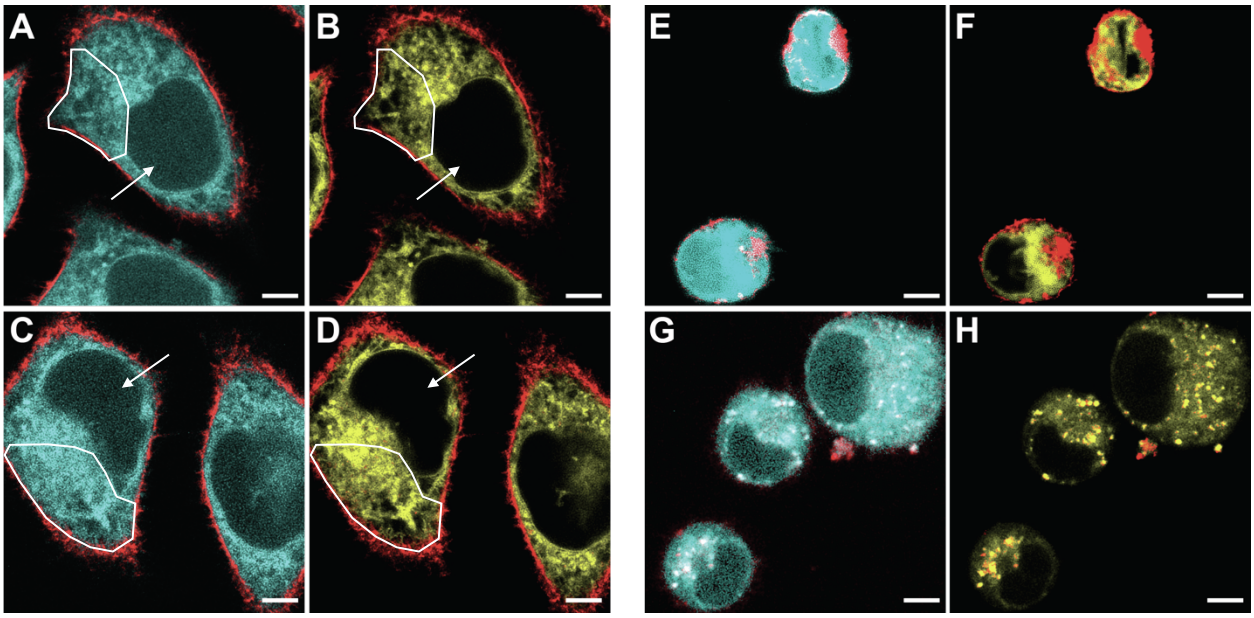

Figure S14. Confocal Images of Live Cells with TEG-TC or TEG-TC-ONOO–, related to Figure 4 and 5

Confocal images of HeLa cells treated with **(A, B) TEG-TC** only or **(C, D)** IFN-γ/LPS/PMA, followed by **TEG-TC-ONOO**$^{-}$, and RAW 246.7 cells treated with **(E, F) TEG-TC** only or **(G, H)** LPS, followed by **TEG-TC-ONOO**$^{-}$. Cell cytoskeleton was assessed with CellMask™ Deep Red Actin Tracking Stain. TEG-TC channel: 405/475 nm. White arrows and polygons **(A–D)** indicate representative locations that highlight signal intensity differences between the TEG-TC and ER channels. Scale bars = 5 μm.

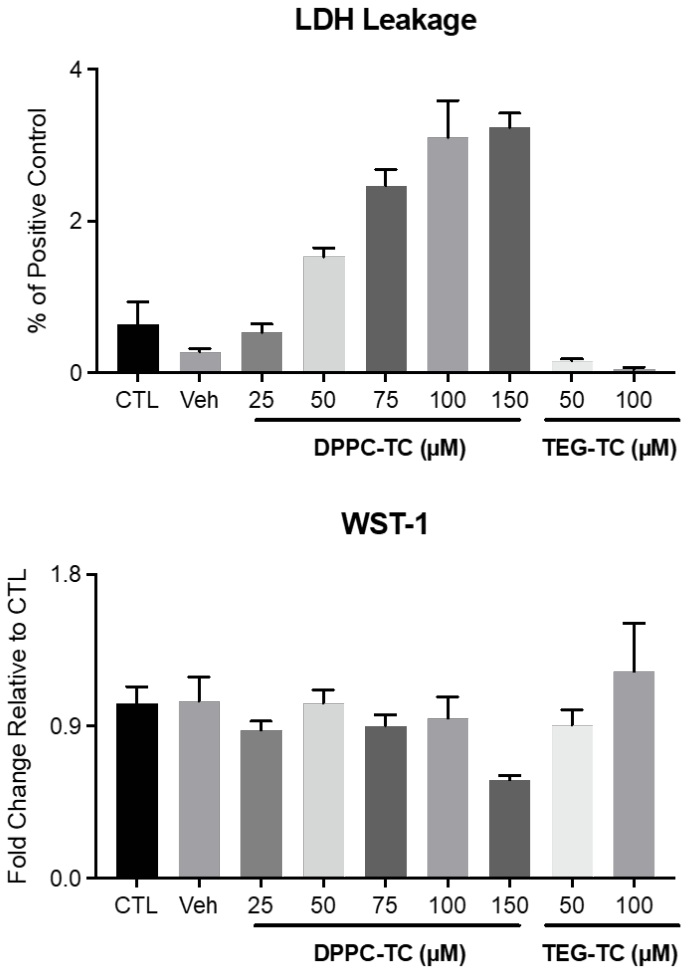

Figure S15. Cellular viability in PCLS using LDH leakage and WST-1 reduction, related to Figure 6

Cytotoxicity of **DPPC-TC** in PCLS. Lung slices were incubated for 1 hour with varying doses of **DPPC-TC** or **TEG-TC** and assessed for viability by measuring LDH release to the medium or WST-1 reduction within the slice using established techniques. LDH activity was measured in the medium using the cytotoxicity detection assay (Roche) using a spectramax spectrophotometer. The quantity of released LDH is expressed as a percentage of LDH in the medium from lysed slices. WST-1 reduction was measured following incubation with Cell Proliferation agent, WST-1 (Roche) and is expressed as a ratio of reduction in untreated slices.

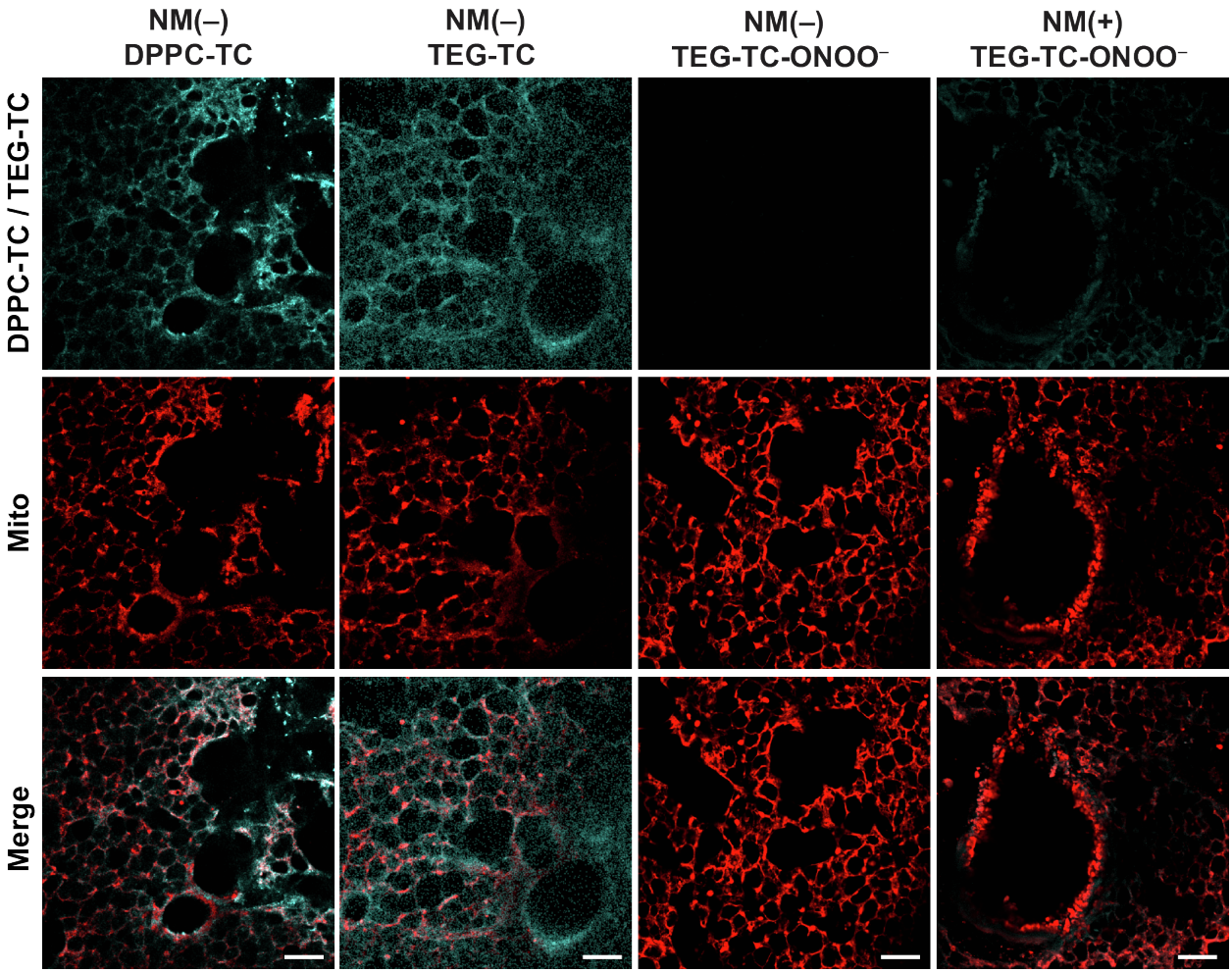

Figure S16. Supporting confocal images of PCLS, related to Figure 6

Confocal images of PCLS incubated with **DPPC-TC** (amphiphile, positive control), **TEG-TC** (non-amphiphile, positive control), or **TEG-TC-ONOO⁻** (non-amphiphilic probe). NM (+): nitrogen mustard exposure. Scale bar = 100 μm. The channel "DPPC-TC/TEG-TC" represents excitation at 405 nm.

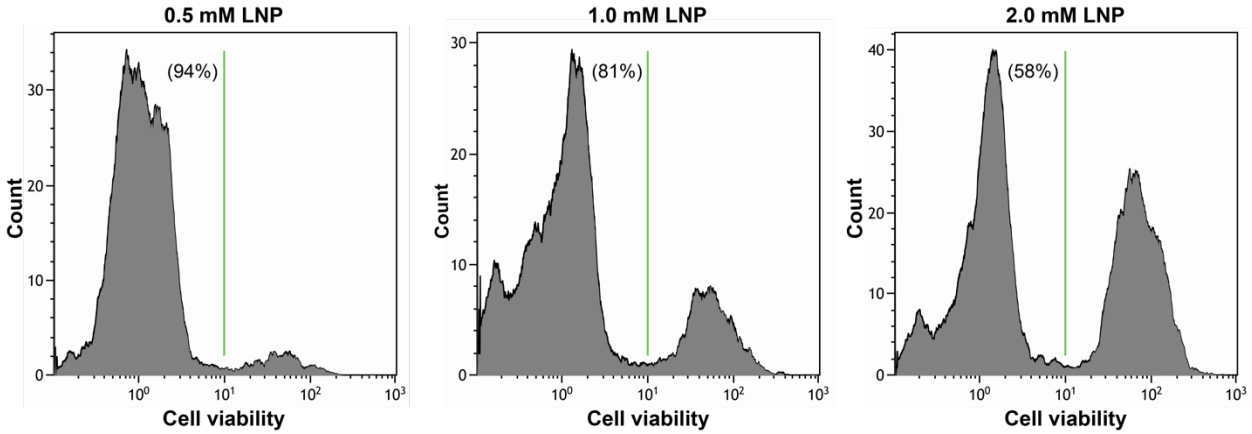

Figure S17. Viability analysis of BAL cells, related to Figure 6

Viability of BAL cells from mice instilled with various concentrations of LNPs.

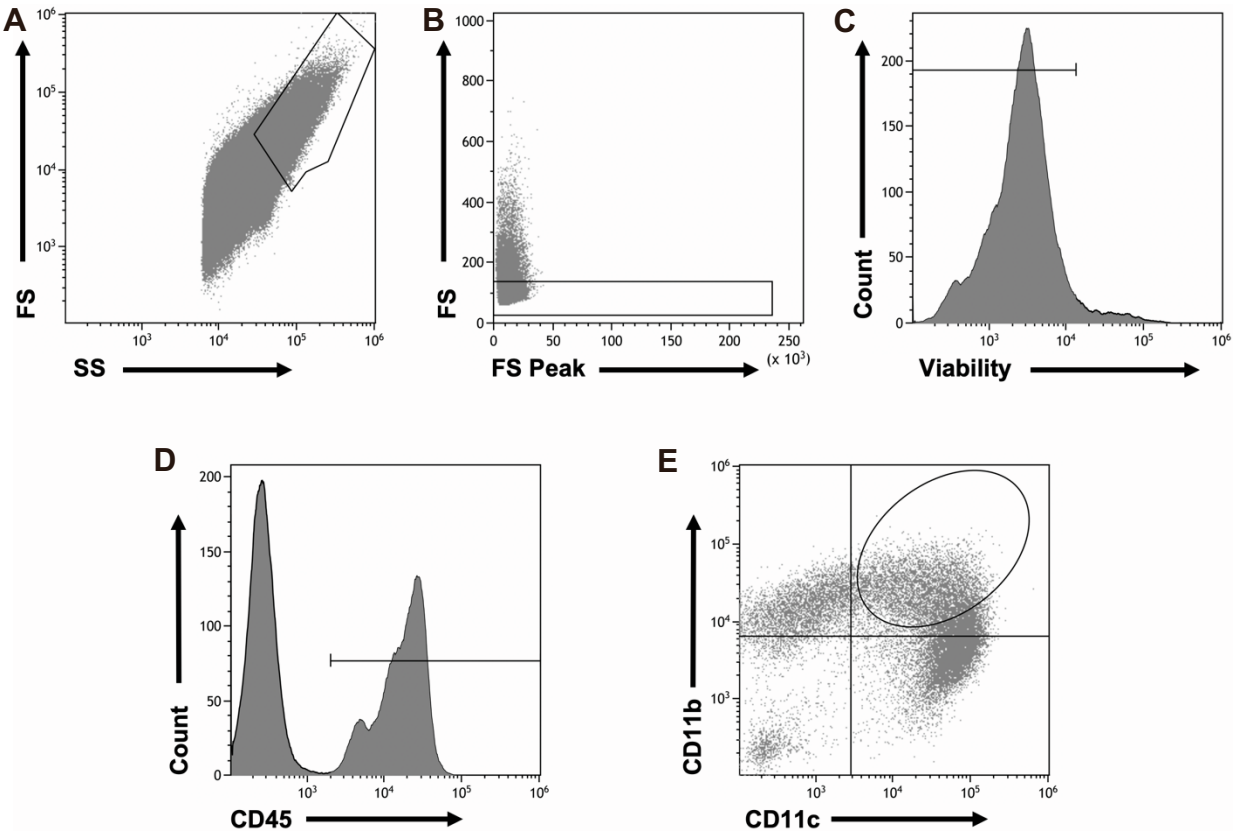

Figure S18. Gating strategy for flow cytometry data, related to Figure 6

Analyses of alveolar macrophages in BAL fluid using flow cytometry. BAL was performed 3 hours post the final LNP instillation. Cells were isolated and immunostained with fluorescent antibodies (CD45, CD11b and CD11c) followed by a viability dye (Fixable Viability Dye eFluor 780). The immunostained BAL samples were analyzed using a Gallios 10-color flow cytometer (Beckman Coulter, CA, USA). The flow cytometry data were analyzed using Kaluza software, and cells were gated based on **(A, B)** size and complexity, **(C)** viability, and **(D)** CD45 positivity. The myeloid lineage was determined based on the positive staining with CD45. **(E)** The CD45+ cells were further analyzed for CD11b and CD11c expression.

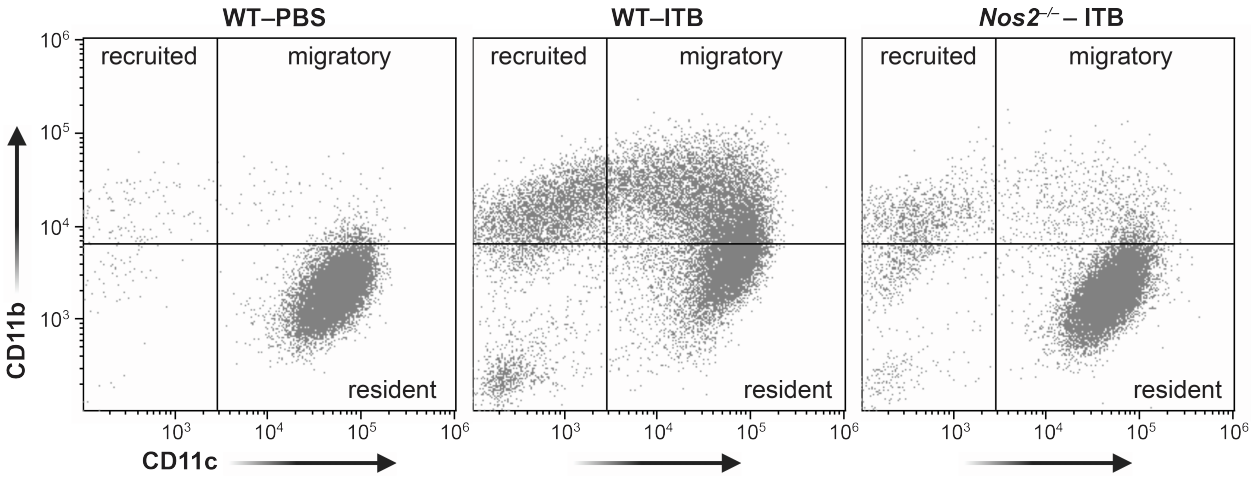

Figure S19. CD11b versus CD11c expression, related to Figure 6

Scatter-plot analyses of CD11b versus CD11c expression in BAL cells.